iScience

CellPress
OPEN ACCESS

Article

AAV-*GRN* partially corrects motor deficits and ALS/FTLD-related pathology in *Tmem106b*$^{-/-}$*Grn*$^{-/-}$ mice

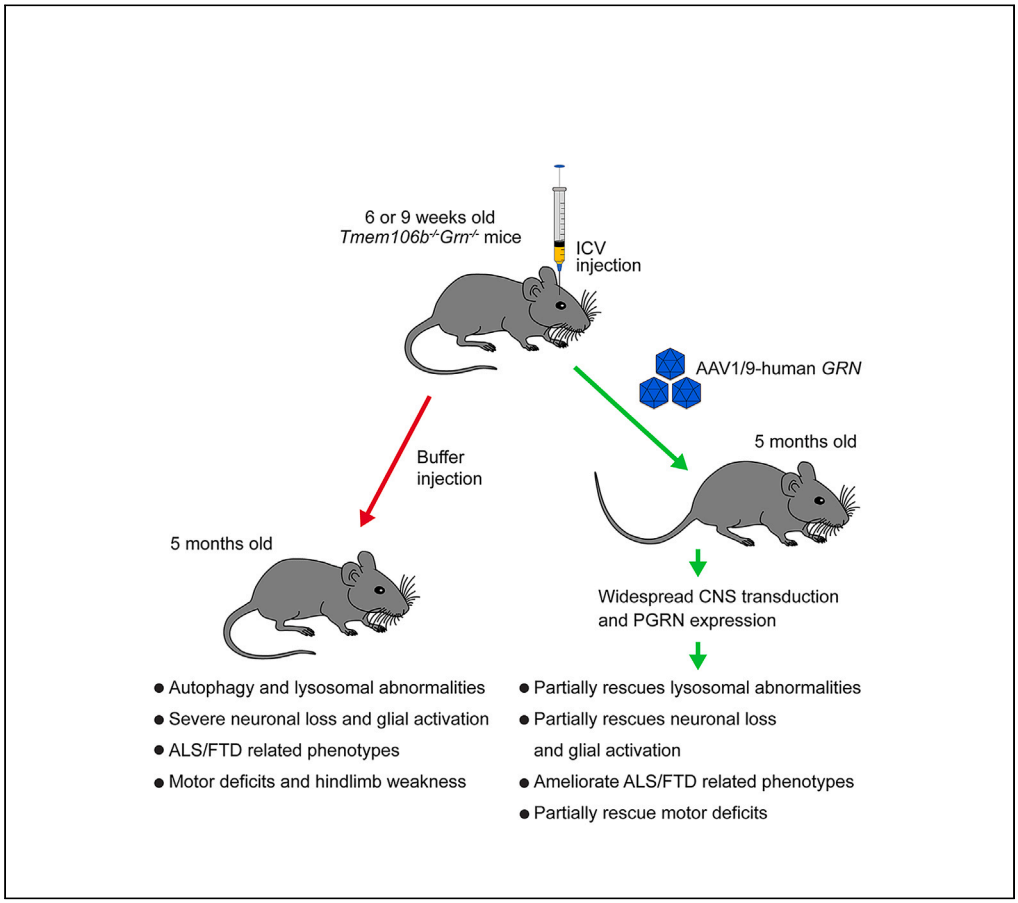

Tuancheng Feng, Gregory Minevich, Pengan Liu, ..., Hua Long, Ananya Mitra, Fenghua Hu

fh87@cornell.edu

Highlights

Tmem106b$^{-/-}$*Grn*$^{-/-}$ mice develop ALS/FTLD related pathology at 2-month-old

ICV injection of AAV1/9-*GRN* viruses leads to widespread CNS expression of *GRN*

AAV1/9-*GRN* partially rescues motor deficits and pathology in *Tmem106b*$^{-/-}$*Grn*$^{-/-}$ mice

Tmem106b$^{-/-}$*Grn*$^{-/-}$ mice are a robust model to test the efficacy of PGRN therapies

Feng et al., iScience *26*, 107247
July 21, 2023
https://doi.org/10.1016/j.isci.2023.107247

iScience

CellPress
OPEN ACCESS

Article

AAV-*GRN* partially corrects motor deficits and ALS/FTLD-related pathology in *Tmem106b*$^{-/-}$*Grn*$^{-/-}$ mice

Tuancheng Feng,[1] Gregory Minevich,[2] Pengan Liu,[1] Henry Xin Qin,[1] Glenn Wozniak,[2] Jenny Pham,[2] Khanh Pham,[2] Akshata Korgaonkar,[2] Michael Kurnellas,[2] Nadine A. Defranoux,[2] Hua Long,[2] Ananya Mitra,[2] and Fenghua Hu[1,3,*]

SUMMARY

Loss of function of progranulin (PGRN), encoded by the *granulin* (*GRN*) gene, is implicated in several neurodegenerative diseases. Several therapeutics to boost PGRN levels are currently in clinical trials. However, it is difficult to test the efficacy of PGRN-enhancing drugs in mouse models due to the mild phenotypes of *Grn*$^{-/-}$ mice. Recently, mice deficient in both PGRN and TMEM106B were shown to develop severe motor deficits and pathology. Here, we show that intracerebral ventricle injection of PGRN-expressing AAV1/9 viruses partially rescues motor deficits, neuronal loss, glial activation, and lysosomal abnormalities in *Tmem106b*$^{-/-}$*Grn*$^{-/-}$ mice. Widespread expression of PGRN is detected in both the brain and spinal cord for both AAV subtypes. However, AAV9 but not AAV1-mediated expression of PGRN results in high levels of PGRN in the serum. Together, these data support using the *Tmem106b*$^{-/-}$*Grn*$^{-/-}$ mouse strain as a robust mouse model to determine the efficacy of PGRN-elevating therapeutics.

INTRODUCTION

Haploinsufficiency of the progranulin (PGRN) protein, due to heterozygous mutations in the *granulin* (*GRN*) gene, is a leading cause of frontotemporal lobar degeneration with TAR DNA-binding protein 43 (TDP-43) aggregates (FTLD-TDP), which is commonly characterized by social and emotional behavior deficits.[1–3] Complete loss of the PGRN protein due to homozygous *GRN* mutations causes neuronal ceroid lipofuscinosis (NCL) type 11, a lysosomal storage disorder with lipofuscin accumulation.[4–6] In addition, PGRN polymorphisms have also been associated with several other neurodegenerative diseases, including Gaucher disease, amyotrophic lateral sclerosis (ALS), Alzheimer's disease (AD), Parkinson's disease (PD), and limbic-predominant age-related transactivation response DNA-binding protein 43 encephalopathies (LATE).[7–12]

PGRN is a widely expressed glycoprotein with important roles in cell proliferation and migration, development, immune function, wound healing, and tumorigenesis.[13] In the central nervous system (CNS), PGRN functions as a neurotrophic factor and promotes neurite outgrowth.[14–18] Growing evidence suggests that PGRN also regulates many microglial activities, including migration, phagocytosis, and synapse pruning.[18–25]

PGRN is comprised 7.5 granulin repeats, and can be either secreted or delivered to the lysosomal compartment.[13,20,26,27] PGRN has been shown to co-traffic to the lysosome with prosaposin (PSAP), the precursor of lysosomal saposin peptides important for glycosphingolipid metabolism.[28–30] Within the lysosome, PGRN is cleaved into a paragranulin and seven, highly conserved, disulfide-bond-containing, granulin peptides by lysosomal proteases.[31–33] Accumulating evidence suggests a critical role of PGRN in the lysosome.[26,27] Transcriptionally, PGRN is regulated by the transcriptional factor EB (TFEB), a master regulator of lysosomal biogenesis and autophagy.[34–36] In mouse models, PGRN-deficiency leads to lysosomal abnormalities, lipofuscin accumulation, and microgliosis.[37,38] Lysosomal phenotypes are also present in FTLD and NCL patients with *GRN* mutations.[39,40] PGRN and granulin peptides have been shown to be critical for the proper regulation of several lysosomal enzymes, including cathepsin D,[14,41–43] and glucocerebrosidase[44–46] and for the maintenance of proper levels of Bis (monoacylglycerol) phosphate (BMP),[47,48] a phospholipid enriched in the endolysosomal compartment.[49]

[1]Department of Molecular Biology and Genetics, Weill Institute for Cell and Molecular Biology, Cornell University, Ithaca, NY 14853, USA

[2]Alector Inc, South San Francisco, CA 94080, USA

[3]Lead contact

*Correspondence: fh87@cornell.edu

https://doi.org/10.1016/j.isci.2023.107247

Since PGRN haploinsufficiency is a leading cause of FTLD, restoring PGRN to normal levels in patients with *GRN* mutations has been sought after as a therapeutic strategy.[12,50,51] Latozinemab, an anti-sortilin antibody currently in phase 3 clinical trials (NCT04374136), is a well-tolerated treatment that restores cerebrospinal fluid (CSF) PGRN to physiological levels in *GRN* mutation carriers. Another approach to elevate PGRN levels in GRN mutation carriers employs recombinant PGRN replacement[48] (NCT05262023). Additionally, recombinant adeno-associated viral (rAAV) vectors expressing human PGRN (hPGRN) are currently in clinical trials to treat FTLD patients with *GRN* mutations (NCT04747431, NCT04408625).

The cellular tropism of the AAV virus depends on several factors, including AAV serotypes and delivery routes.[52] Mouse and non-human primates (NHP) rhesus macaque models have been used in testing the efficacy of AAV-mediated PGRN expression. Targeted delivery into the medial prefrontal cortex (mPFC) of mouse PGRN expressing rAAV2 viruses normalized prefrontal cortical lysosomal protein levels and reversed social dominance deficits of 11–12-month-old $Grn^{+/-}$ mice,[53] and rescued lysosomal abnormalities and reduced lipofuscinosis and microgliosis in 10–12-month-old $Grn^{-/-}$ mice.[54] Delivery of hPGRN expressing AAVhu68 (an AAV9 variant) viruses into the lateral cerebral ventricle also reversed brain lysosomal abnormalities and lipofuscin deposits, and completely corrected microgliosis in aged $Grn^{-/-}$ mice.[55] In addition, PGRN expression mediated by AAV serotypes 1, 5, and hu68 through direct intra-cisterna magna (ICM) delivery has also been shown to elevate PGRN levels in the CSF in rhesus macaques.[55] T cell infiltration and neurotoxicity are a common concern for AAV-mediated gene therapy[56,57] and have been reported in one study with AAV9-mediated hPGRN delivery into the posterior right lateral ventricle in *GRN* knockout mice.[58] Mild axonal degeneration of sensory neurons in the spinal cord has also been observed in the non-human primate model with AAV-PGRN delivery.[55]

However, despite exhibiting lipofuscinosis, lysosomal deficits, and microgliosis when aged to 7–9 months old, PGRN-deficient mice do not exhibit neuronal loss and obvious behavioral deficits.[37] Thus, animal models with better predictive validity would be of particular importance in drug development programs targeting PGRN dysfunction.

TMEM106B, originally discovered as a risk factor for FTLD with *GRN* mutations,[59–63] encodes a type II lysosomal transmembrane protein.[64–66] TMEM106B affects several aspects of lysosomal functions, including lysosomal morphology and function,[64–67] lysosome pH,[65,68–70] lysosome exocytosis,[69] lysosomal positioning within the cell,[71] lysosome trafficking in neuronal dendrites,[72] and lysosomal trafficking across the axon initial segment (AIS).[73,74] In mouse models, TMEM106B deficiency leads to mild myelination deficits,[71,75] microglial survival defects in response to demyelination,[70] reduced survival of Purkinje cells during aging, and mild motor coordination defects.[76–78]

Since PGRN and TMEM106B regulate different aspects of lysosome functions,[26,27,79] it is not surprising that loss of both PGRN and TMEM106B results in severe lysosomal abnormalities, motor dysfunction, neuronal loss, glial activation, and FTLD-related pathology in mice.[73,80,81] Importantly, these mice exhibit motor defects as early as 2.5 months old and progress with age, resulting in an early death at around 5 months old.[73,80,81] Since TMEM106B deficiency alone in mice only leads to mild phenotypes,[79] these findings suggest that $Tmem106b^{-/-}Grn^{-/-}$ mice could be used as a novel preclinical mouse model to test the efficacy of PGRN therapy. Here, we report that hPGRN expression mediated by intracerebral ventricle (ICV) delivery of AAV1 or AAV9 viruses partially rescues motor deficits, neuronal loss, glial activation, and lysosomal abnormalities in $Tmem106b^{-/-}Grn^{-/-}$ mice. Our study shows that the $Tmem106b^{-/-}Grn^{-/-}$ mouse strain can be used as a robust mouse model to determine the efficacy of PGRN therapies.

RESULTS

$Tmem106b^{-/-}Grn^{-/-}$ mice show pathological changes at 2 months of age

Since $Tmem106b^{-/-}Grn^{-/-}$ mice start to exhibit obvious ataxia, hindlimb weakness, and motor defects at 2.5 months of age, with the spinal cord having more severe pathological changes compared to other brain regions,[73] we first assayed the lysosome phenotypes and protein aggregation in the spinal cord from 2-month-old $Tmem106b^{-/-}Grn^{-/-}$ mice. We observed a significant increase of lysosomal enzyme cathepsin D (Cath D) in the RIPA-soluble fraction, and a dramatic accumulation of ubiquitinated proteins and autophagy adaptor protein p62 in the RIPA-insoluble, but urea-soluble fraction from the spinal cord of $Tmem106b^{-/-}Grn^{-/-}$ mice at 2 months of age (Figures 1A and 1B), suggesting significant lysosomal defects and ALS/FTLD-related pathological changes appearing in 2-month-old $Tmem106b^{-/-}Grn^{-/-}$ mice.

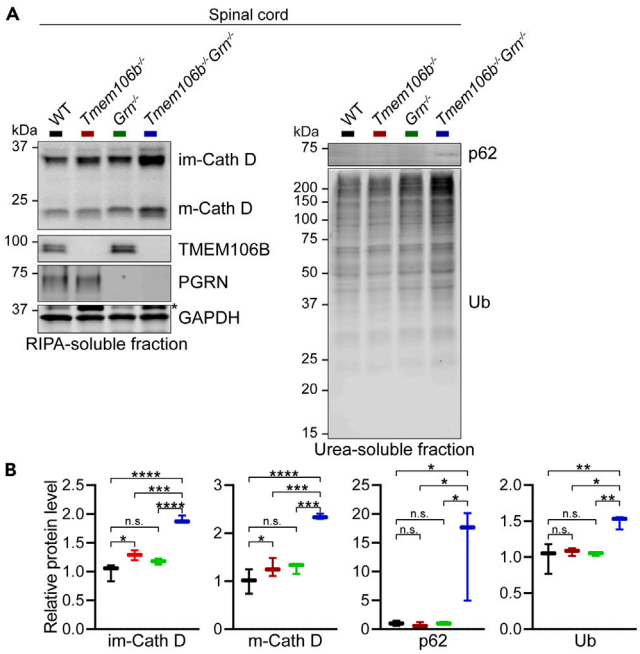

Figure 1. Lysosomal defects and ALS/FTLD-related pathological changes in the spinal cord of 2-month-old *Tmem106b*$^{-/-}$*Grn*$^{-/-}$ mice

(A and B) Western blot analysis of the protein levels of lysosomal enzyme cathepsin D (Cath D), TMEM106B, PGRN, and GAPDH in RIPA-soluble fractions, and ubiquitinated proteins and p62 in urea-soluble fractions of the spinal cord from 2-month-old WT, *Tmem106b*$^{-/-}$, *Grn*$^{-/-}$, and *Tmem106b*$^{-/-}$*Grn*$^{-/-}$ mice. The asterisk indicates non-specific bands. n = 3. Data are presented as mean ± SEM. One-way ANOVA tests with Tukey's multiple comparisons: *, $p < 0.05$, **, $p < 0.01$, ***, $p < 0.001$, ****, $p < 0.0001$; ns, no significance.

AAV1/9-mediated human PGRN expression in *Tmem106b*$^{-/-}$*Grn*$^{-/-}$ mice

Numerous studies have shown that rAAV vectors are a promising platform to offer stable, efficient, non-cytotoxic, and non-integrated gene delivery to treat different neurodegenerative diseases.[82–85] To achieve ubiquitous, strong, constitutive, and long-term expression of hPGRN, we cloned the human *GRN* gene under the eukaryotic translation elongation factor 1 α (EF-1α) promoter into the single-stranded AAV (ssAAV) vector (Figure 2A). In consideration of the differential behavior of AAV serotypes in the extent of viral spreading, cell type specificity, and transduction efficiency, the ssAAV vector containing the human *GRN* gene was packaged into AAV1 or AAV9 capsids (AAV1-*GRN* or AAV9-*GRN*).

To determine the efficacy of AAV-mediated PGRN expression in *Tmem106b*$^{-/-}$*Grn*$^{-/-}$ mice, hPGRN expressing AAV viruses (1.2×10^{11} viral genome particles/mouse) was administered to 6- or 9-week-old *Tmem106b*$^{-/-}$*Grn*$^{-/-}$ mice via intracerebroventricular (ICV) injections (Figure 2B). Fifteen or twelve weeks after injection, we examined AAV1- or AAV9-*GRN* transduction in 5-month-old *Tmem106b*$^{-/-}$*Grn*$^{-/-}$ mice. To examine the transduction efficacy and the expression of hPGRN in CNS, human-specific PGRN ELISA was carried out using frontal cortex, spinal cord lysates, and serum. Overall, hPGRN expression was successfully detected in the frontal cortex (Figure 3A) and spinal cord (Figure 3B) lysates from *Tmem106b*$^{-/-}$*Grn*$^{-/-}$ mice injected with AAV1- or AAV9-*GRN* at 6-week-of-age or 9-week-of-age. Despite variability between individual mice, AAV9-*GRN* had relatively higher levels of expression than AAV1-*GRN*, although not statistically significant (Figures 3A and 3B). Interestingly, high hPGRN levels were detected in the terminal serum from *Tmem106b*$^{-/-}$*Grn*$^{-/-}$ mice injected with AAV9-*GRN* at 6- and 9-week-of-age (~470 ng/mL), similar to the levels of endogenous PGRN in the serum of normal WT mice,[86] but not from AAV1-*GRN* injected mice (Figure 3C). To further analyze the expression and distribution of hPGRN in CNS, we performed immunostaining in brain and spinal cord sections using a human-specific PGRN antibody (Figures 3D and S1). hPGRN signals were detected in the neurons in the cortical layer 2/3 in frontal cortex and spinal cord sections (Figure 3D) and other regions in the brain (Figures S1A and S1B) from the *Tmem106b*$^{-/-}$*Grn*$^{-/-}$ mice injected with AAV1- or AAV9-*GRN*. In addition, PGRN signals were also detected in GFAP-positive astrocytes and a small population of IBA1-positive microglia in both AAV1- and AAV9-*GRN* infected

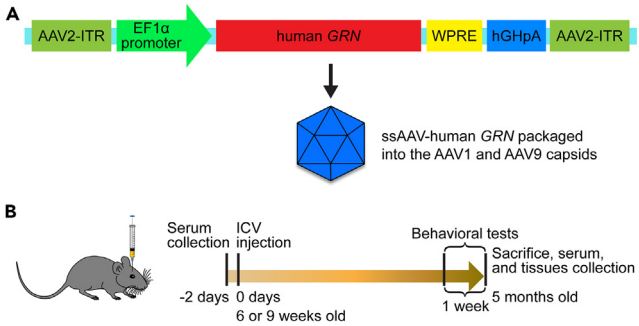

Figure 2. Experimental design and timeline

(A) Diagram of the single-stranded AAV (ssAAV) vector containing the human *GRN* gene under the eukaryotic translation elongation factor 1 α (EF-1α) promoter flanked by AAV2-ITRs. The ssAAV-*GRN* was packaged within AAV serotypes 1 or 9. (B) Timeline of the study. Serum collected from all the mice 2 days before injection was used as the negative control. 6- or 9-week-old *Tmem106b*$^{-/-}$*Grn*$^{-/-}$ mice were intracerebroventricularly (ICV) injected the hPGRN expressing AAV1 or AAV9 viruses. Behavioral tests were preformed within 1 week before sacrificing the mice. Terminal serum, brain, and spinal cord tissues from all the mice were collected at 5 months of age.

mice (Figures 3D and S1B). Efficient transduction and high hPGRN expression in ventricle and spinal ependymal cells has also been observed in *Tmem106b*$^{-/-}$*Grn*$^{-/-}$ mice treated with either AAV1- or AAV9-*GRN* (Figures 3E and S1A). Together, these results suggested that AAV1/9-*GRN* delivered by intracerebroventricular injection achieved efficient transduction, and achieved sufficient and widespread expression of hPGRN in the brain and spinal cord in the *Tmem106b*$^{-/-}$*Grn*$^{-/-}$ mice.

AAV1/9-mediated hPGRN expression partially rescues motor deficits in *Tmem106b*$^{-/-}$*Grn*$^{-/-}$ mice

Since *Tmem106b*$^{-/-}$*Grn*$^{-/-}$ mice exhibit severe hindlimb weakness and motor dysfunction,[73,80,81] behavioral tests were carried out to examine motor function following intracerebroventricular AAV1- or AAV9-*GRN* injection. Compared to the mice injected with buffer control, we observed a significant improvement of motor activities in *Tmem106b*$^{-/-}$*Grn*$^{-/-}$ mice receiving the AAV1- or AAV9-*GRN* injection at 6-week-of-age as shown in the open field test, but not in the mice treated at 9-week-of-age (Figures 4A and 4B). Moreover, AAV1- and AAV9-*GRN* treated *Tmem106b*$^{-/-}$*Grn*$^{-/-}$ mice had quicker righting reflex and spent much less time rolling over when flipped to a supine position (Figure 4C) (Videos S1, S2, and S3) and showed a significant increase in stride length in footprint analysis (Figure 4D), indicating an improvement in motor coordination. However, abnormal hindlimb clasping behavior was still observed in mice injected with AAV1- or AAV9-*GRN* (Figure S2). Since hindlimb clasping defects could be caused by deficits in the spinal cord, cerebellum, basal ganglia, or neocortex,[87] it is likely that some of these regions do not receive enough AAV-*GRN* viruses to mediate PGRN expression due to limited virus spreading. Nevertheless, our results demonstrated that AAV1- or AAV9-mediated expression of hPGRN in *Tmem106b*$^{-/-}$*Grn*$^{-/-}$ mice significantly, but not completely rescued hindlimb weakness and motor dysfunction.

AAV1/9-mediated hPGRN expression partially ameliorates neuropathology in the spinal cord of *Tmem106b*$^{-/-}$*Grn*$^{-/-}$ mice

Since *Tmem106b*$^{-/-}$*Grn*$^{-/-}$ mice exhibit a severe neuronal loss in the spinal cord,[73,80,81] we examined the numbers of neurons in the spinal cord from 5-month-old WT and *Tmem106b*$^{-/-}$*Grn*$^{-/-}$ mice injected with buffer control, AAV1-*GRN* or AAV9-*GRN*. A significant rescue in the numbers of NeuN-positive neurons in the spinal cord sections was observed in AAV1- or AAV9-*GRN* injected *Tmem106b*$^{-/-}$*Grn*$^{-/-}$ mice treated at 6-week-of-age (not in mice at 9-week-of-age due to the variabilities between individual mice), but not in mice receiving buffer control (Figures 5A and 5B). Previously, we have shown that motor neurons are selectively affected by the loss of both TMEM106B and PGRN in mice.[73] This loss of motor neurons is completely rescued by AAV1/9-mediated hPGRN expression, as shown by immunostaining with antibodies against choline acetyltransferase (ChAT) in the ventral horn region of the spinal cord (Figures 5C and 5D).

In addition, loss of TMEM106B and PGRN in mice results in excessive activation of microglia and astrocytes.[73,80,81] Significantly decreased intensities of GFAP, a marker for astrocytes, and CD68, a marker for activated microglia, were observed in spinal cord sections of *Tmem106b*$^{-/-}$*Grn*$^{-/-}$ mice treated with

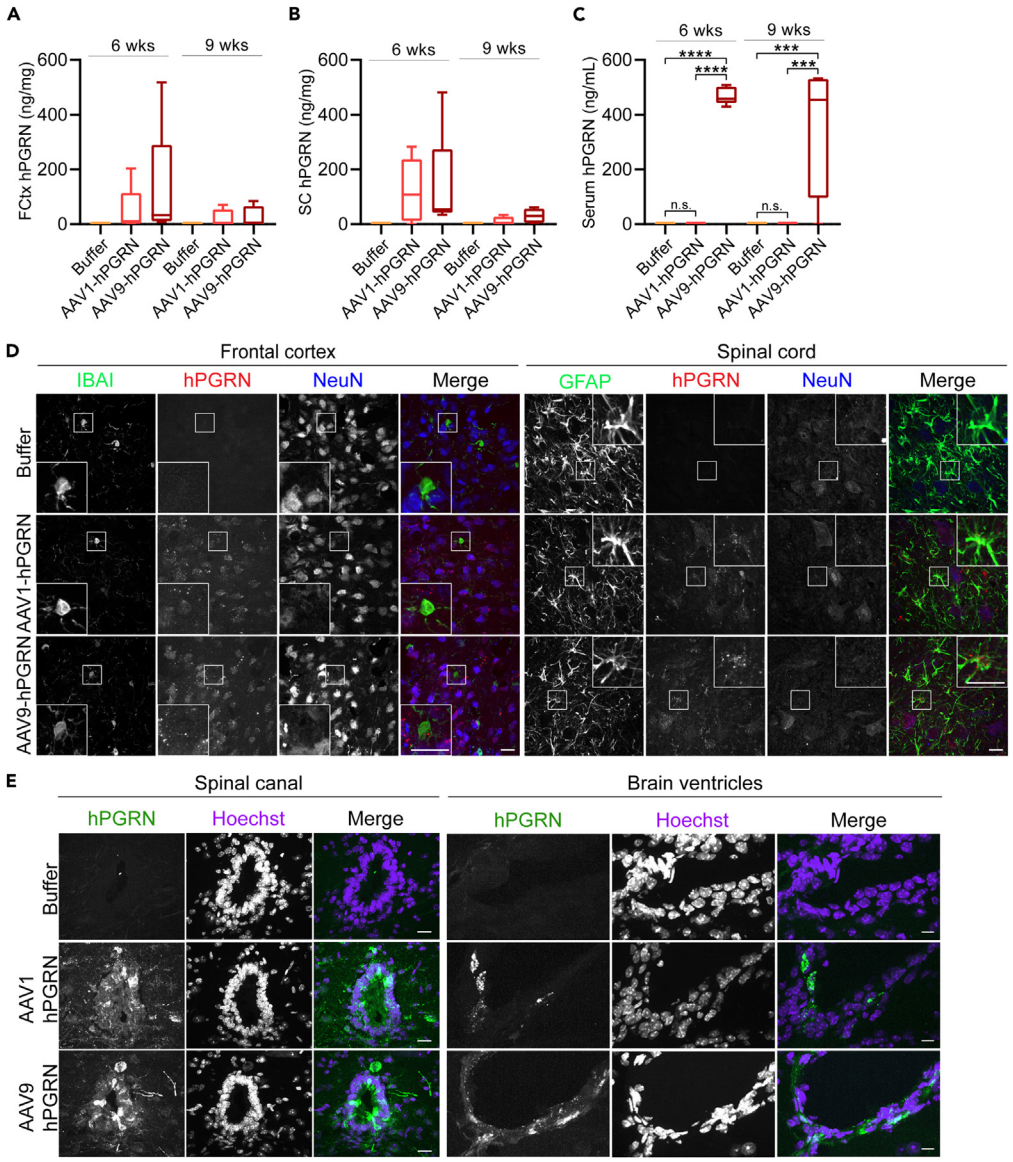

Figure 3. Efficient transduction of AAV1/9-*GRN* viruses following intracerebroventricular AAV1/9-*GRN* injection

(A–C) Human PGRN in the frontal cortex (FCtx) (A), spinal cord (SC) (B), and serum (C) lysates from 5-month-old WT or *Tmem106b*$^{-/-}$*Grn*$^{-/-}$ mice injected with buffer control, AAV1-*GRN* or AAV9-*GRN* were measured by ELISA assay (n = 4–5). Data are presented as mean ± SEM. One-way ANOVA tests with Tukey's multiple comparisons: ***, $p < 0.001$, ****, $p < 0.0001$; ns, no significance.

(D) Brain sections from 5-month-old mice injected with buffer control or AAV-*GRN* viruses at 9 weeks of age were stained with NeuN, IBA1, and hPGRN antibodies, and Hoechst. Sinal cord sections (C1-C4) from 5-month-old mice injected with buffer control or AAV-*GRN* viruses at 6 weeks of age were stained with NeuN, GFAP, and hPGRN antibodies, and Hoechst. Scale bar: 20 μm.

(E) Brain and spinal cord sections (C1-C4) from 5-month-old mice injected with buffer control or AAV-*GRN* viruses at 6 weeks of age were stained with anti-hPGRN antibodies and Hoechst. Scale bar: 20 μm for brain ventricles, and 10 μm for spinal canal.

AAV1- or AAV9-*GRN* compared to mice injected with buffer control (Figures 6A and 6B). Analysis of microglial morphology in the spinal cord revealed a significant increase in the number of microglia processes in AAV1- or AAV9-*GRN* treated *Tmem106b*$^{-/-}$*Grn*$^{-/-}$ mice (Figures 6C and 6D), indicating a reduced microglia activation with restored PGRN expression. In addition, the protein levels of GFAP were significantly reduced in the frontal cortical lysates of *Tmem106b*$^{-/-}$*Grn*$^{-/-}$ mice receiving the AAV1- or AAV9-*GRN*

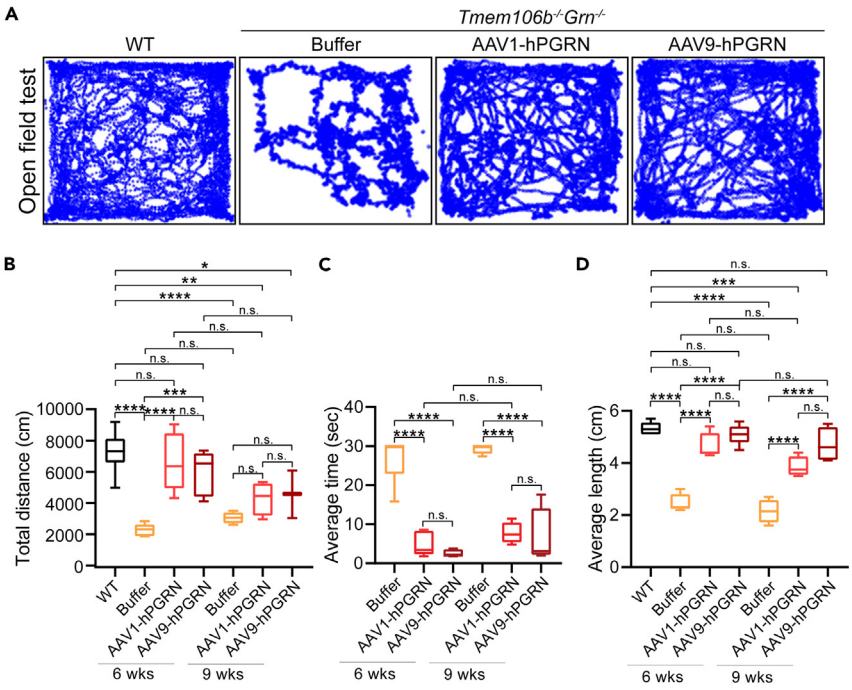

Figure 4. AAV1/9-*GRN* mediated PGRN expression partially rescues motor deficits in *Tmem106b*$^{-/-}$*Grn*$^{-/-}$ mice

(A and B) Representative images of mouse tracing in open field test from 4.75-month-old WT or *Tmem106b*$^{-/-}$*Grn*$^{-/-}$ mice injected with buffer control, AAV1-*GRN* or AAV9-*GRN* at 6 weeks of age (A). The total movement was quantified. n = 3–12. Data are presented as mean ± SEM. One-way ANOVA tests with Tukey's multiple comparisons: *, $p < 0.05$, **, $p < 0.01$, ***, $p < 0.001$, ****, $p < 0.0001$; ns, no significance.

(C) The time for mice to flip back was quantified in the rolling-over test. n = 4–6. Data are presented as mean ± SEM. One-way ANOVA tests with Tukey's multiple comparisons: ****, $p < 0.0001$; ns, no significance.

(D) The stride length is quantified in the footprint test. n = 4–6. Data are presented as mean ± SEM. One-way ANOVA tests with Tukey's multiple comparisons: ***, $p < 0.001$, ****, $p < 0.0001$; ns, no significance.

injection at 6-week-of-age, but not in the mice treated at 9-week-of-age (Figures S3). No significant difference was observed in CD68 signals in the brain sections in either group, which might be due to the variabilities in the volumetric spread of AAV viruses in the brain between individual mice (data not shown).

AAV1/9-mediated hPGRN expression partially rescue lysosomal defects in the spinal cord of *Tmem106b*$^{-/-}$*Grn*$^{-/-}$ mice

Numerous evidence suggests that both PGRN and TMEM106B play important and non-overlapping roles in proper lysosomal function.[26,27,73,79–81] Deletion of both TMEM106B and PGRN in mice results in severe lysosome abnormalities, including lipofuscin accumulation and upregulation of lysosomal proteins.[73,80,81] We found a significant decrease in lipofuscin signals (Figures 7A and 7B) and levels of lysosome proteases cathepsin D (Cath D) (Figures 7C and 7D) in the spinal cord of *Tmem106b*$^{-/-}$*Grn*$^{-/-}$ mice treated with AAV1- or AAV9-*GRN* compared to the mice treated with buffer control. However, no obvious difference was detected in lipofuscin signal in the thalamus (data not shown) and in protein levels of CathD in the frontal cortical lysates from AAV1- or AAV9-*GRN* and buffer control injected *Tmem106b*$^{-/-}$*Grn*$^{-/-}$ mice (Figure S3). These results indicated a partial rescue of lysosome defects in *Tmem106b*$^{-/-}$*Grn*$^{-/-}$ mice following AAV1/9-*GRN* injection.

AAV1/9-mediated hPGRN expression partially rescues ALS/FTLD-related pathology in *Tmem106b*$^{-/-}$*Grn*$^{-/-}$ mice

The accumulation of ubiquitin-positive aggregates, autophagy adaptor protein p62, and phosphorylated TDP-43 deposits is a hallmark of ALS/FTLD.[39] These pathological features were observed in the spinal cord of 2-month-old (Figures 2A and 2B) and 5-month-old *Tmem106b*$^{-/-}$*Grn*$^{-/-}$ mice.[73,80,81] A reduction in levels of ubiquitinated proteins, p62 and phosphorylated TDP-43 (S409/S410) deposits in the spinal cord

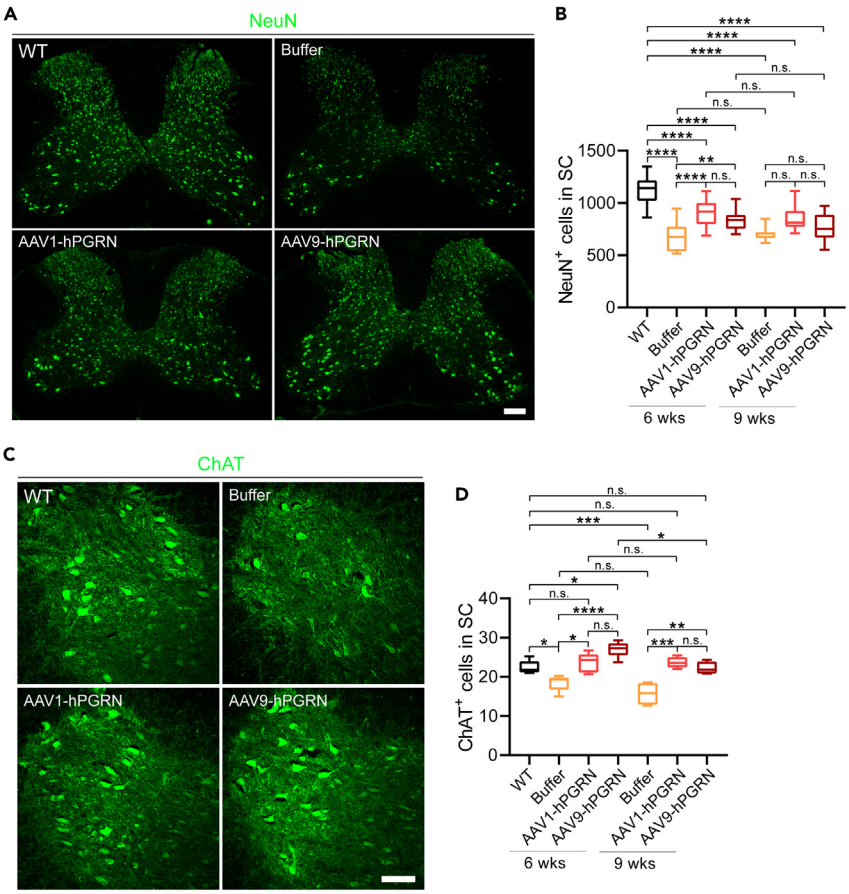

Figure 5. AAV1/9-mediated PGRN expression partially ameliorates neuronal loss in the spinal cord of *Tmem106b*$^{-/-}$*Grn*$^{-/-}$ mice

Representative images of spinal cord sections (C1-C4) from 5-month-old WT or *Tmem106b*$^{-/-}$*Grn*$^{-/-}$ mice injected with buffer control or AAV-*GRN* viruses at 6 weeks of age were stained with NeuN (A) or ChAT (C) antibodies. The numbers of NeuN- and ChAT-positive neurons were quantified (B, D). 3 sections/mouse and 3–6 mice were analyzed for quantification. Data are presented as mean ± SEM. One-way ANOVA tests with Tukey's multiple comparisons: *, $p < 0.05$, **, $p < 0.01$, ***, $p < 0.001$, ****, $p < 0.0001$; ns, no significance. Scale bar: 100 μm (A); 20 μm (C).

(Figures 8A, 8B, and S4) was detected in *Tmem106b*$^{-/-}$*Grn*$^{-/-}$ mice treated with AAV1- or AAV9-*GRN* at 6-week-of-age compared to buffer control, although not to the levels of WT mice. In the cortex, we also detected a reduction in the levels of ubiquitinated proteins and p62 in *Tmem106b*$^{-/-}$*Grn*$^{-/-}$ mice treated with AAV1- or AAV9-*GRN* at 6-week-of-age (Figure S4). However, there is no significant change observed in the mice treated at 9-week-of-age due to the variabilities between individual mice. Together, these data suggest that PGRN expression mediated by AAV1/9-*GRN* partially rescues the ALS/FTLD-related pathology in *Tmem106b*$^{-/-}$*Grn*$^{-/-}$ mice.

DISCUSSION

Tmem106b$^{-/-}$*Grn*$^{-/-}$ mice as a mouse model to test PGRN therapeutics

Since PGRN loss of function has been linked to many neurodegenerative diseases, elevating PGRN levels and functions has been considered as a therapeutic approach for FTLD and other diseases with PGRN deficiency.[12,50,51] Although PGRN haploinsufficiency results in FTLD in humans, PGRN-haploinsufficient mice exhibit minimal phenotypes,[37,53,89] and PGRN-deficient mice only show limited phenotypes during aging, including lipofuscinosis, lysosomal deficits, and microgliosis.[37,38] Thus, it is critical to develop a new mouse model to test the efficacy of therapeutic drugs targeting PGRN. Recently, we and other groups found that deletion of both PGRN and TMEM106B in mice leads to reduced motor activity, hindlimb weakness, and altered clasping behavior.[73,80,81] Severe lysosomal abnormalities, neuronal loss, and glial activation were

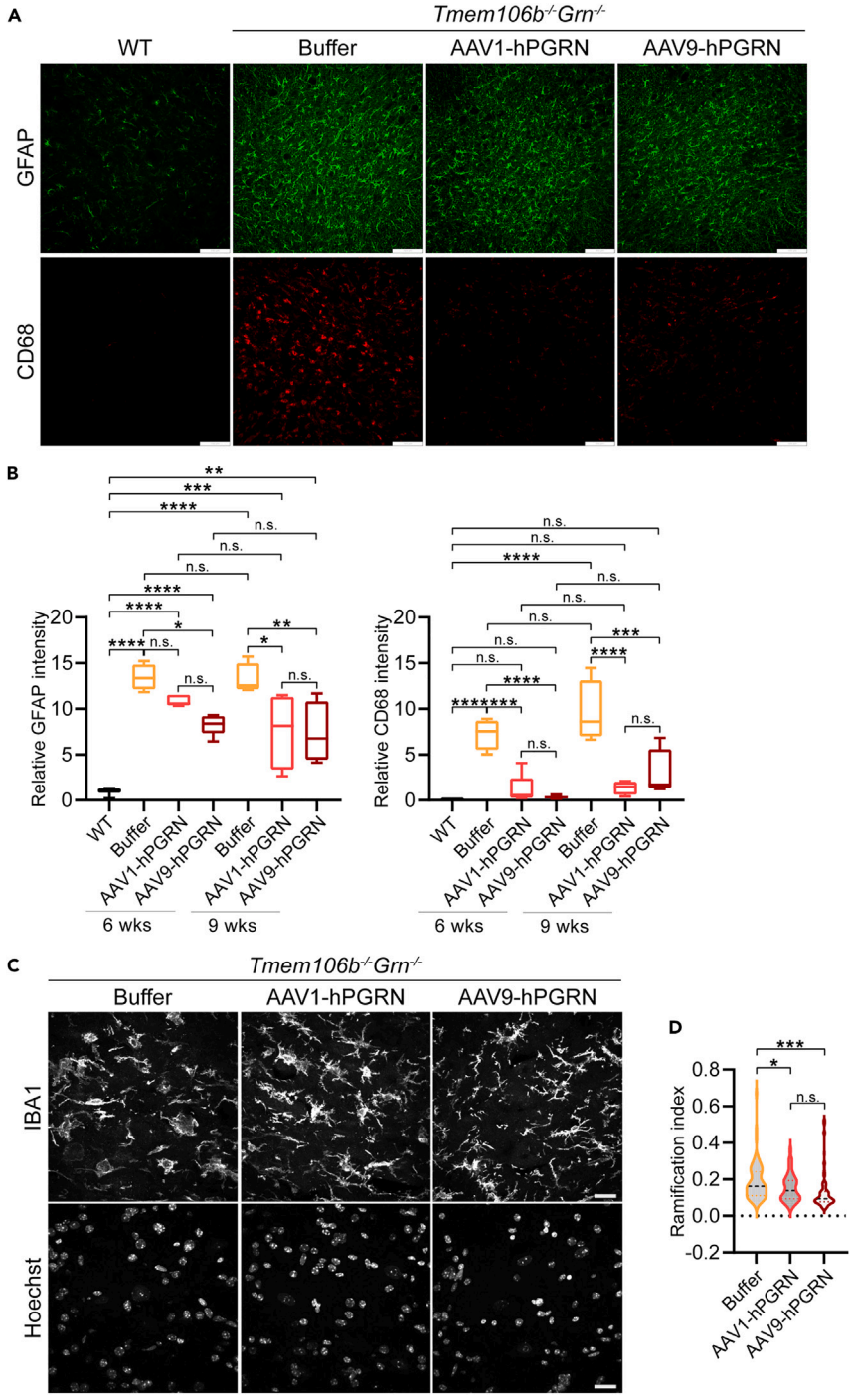

Figure 6. AAV1/9-mediated PGRN expression partially ameliorates glia activation in the spinal cord of *Tmem106b*$^{-/-}$*Grn*$^{-/-}$ mice

(A and B) Representative fluorescence images of spinal cord sections (C1-C4) from 5-month-old WT or *Tmem106b*$^{-/-}$*Grn*$^{-/-}$ mice injected with buffer control or AAV1/9-*GRN* viruses at 6 weeks of age were stained with GFAP or CD68 antibodies (A), and the intensity of GFAP or CD68 were quantified (B). 3–5 sections/mouse were used for quantification. n = 4–6. Data are presented as mean ± SEM. One-way ANOVA tests with Tukey's multiple comparisons: *, $p < 0.05$, **, $p < 0.01$, ***, $p < 0.001$, ****, $p < 0.0001$; ns, no significance. Scale bar: 100 μm.

(C and D) High magnification images from the spinal cord sections (C1-C4) from 5-month-old *Tmem106b*$^{-/-}$*Grn*$^{-/-}$mice injected with buffer control or AAV1/9-*GRN* at 6 weeks of age were stained with IBA1 antibody and Hoechst. The

Figure 6. *Continued*
ramification index (RI = 4π × cell area/[cell perimeter]^2) was used to quantify the microglia shape in microglia morphometric analysis. 1 = a perfectly round cell. RI is smaller than 1 if morphology deviates from perfectly circular and RI is close to zero when the cell is ramified.[88] 80–100 cells/genotype were analyzed. n = 3. Data are presented as mean ± SEM. One-way ANOVA tests with Tukey's multiple comparisons: *, $p < 0.05$, ***, $p < 0.001$; ns, no significance. Scale bar: 20 μm.

observed both in the spinal cord and brain.[73,80,81] More importantly, the motor defects in the *Tmem106b*$^{-/-}$*Grn*$^{-/-}$ mice were observed as early as 2.5 months and progressed with age.[73] A significant increase in the protein levels of lysosomal enzymes, and accumulation of ubiquitinated proteins and p62 were detected in the spinal cord of *Tmem106b*$^{-/-}$*Grn*$^{-/-}$ mice at 2 months of age (Figure 1). The severe motor defects and pathological changes in young *Tmem106b*$^{-/-}$*Grn*$^{-/-}$ mice make them a robust mouse model to test the efficacy of PGRN targeting drugs. Our studies with hPGRN expressing AAV1 or AAV9 viruses in these mice clearly demonstrate the advantages of using these mice to test the efficacy of AAV-mediated human *GRN* gene therapy at the behavioral, pathological, molecular, and cellular levels.

AAV-mediated gene therapy for FTLD-*GRN*

rAAV viruses have been shown to mediate stable, efficient, non-cytotoxic, and non-integrated gene delivery. rAAV-mediated gene therapies are in clinical trials for several neurodegenerative diseases.[82–85] The cellular tropism of AAV depends on several factors, including AAV serotypes and delivery routes.[52] The promoter used to drive gene expression also has been shown to have a big effect on gene therapy efficacy.[90]

Several AAV-*GRN* constructs have been tested in rodent models of PGRN deficiency. In the first study of AAV-mediated *GRN* gene therapy in mice, the chicken β–actin (CBA) promoter in an AAV2 vector was used to drive the expression of mouse *Grn* gene fused with a C-terminal Myc tag.[53,54] AAV2-PGRN was shown to reverse social dominance deficits of 11–12-month-old *Grn*$^{+/-}$ mice,[53] and rescue lysosomal abnormalities and reduce lipofuscinosis and microgliosis in 10–12-month-old *Grn*$^{-/-}$ mice,[54] despite the interference of PGRN binding to sortilin by C-terminal tagging.[91] Moreover, AAV2 does not spread as far from the injection site and has lower transduction levels as compared to AAV1 and AAV9.[84] In subsequent studies, AAV9-mediated human *GRN* expression was chosen to correct phenotypes associated with PGRN deficiency, either driven by a cytomegalovirus (CMV) promoter[58] or a CBA promotor with a CMV early enhancer, chimeric intron, and rabbit beta-globin polyadenylation sequence.[55] However, the CMV early enhancer/chicken β actin (CAG), CMV, and ubiquitously expressing human ubiquitin C promoter (UbiC) promoter has been found to be associated with toxicity and inflammation when delivered via AAV to the mouse eyes,[92] and CMV promoter-mediated gene expression is known to decrease over time due to transcriptional silencing caused by DNA methylation.[93–98] The CBA promoter drives mostly ubiquitous and high neural expression of target genes, but expression tends to be lower in motor neurons.[90]

In consideration of these different factors, the EF-1α promoter which has been shown to have a higher resistance to transcriptional silencing than viral promoters and drive effective transgene expression in mice,[99,100] rats,[101] and in non-human primates,[102,103] was used in our study to drive the expression of human *GRN* gene in order to achieve ubiquitous, safe, strong, constitutive, and long-term expression.[104–106] The ssAAV vector containing the human *GRN* gene was further packaged into AAV1 or AAV9 capsids due to its advantages over other AAVs, including wide spreading from the site of injection, transduction at high levels and with multiple cell types (such as neurons and astrocytes), anterograde, retrograde, and *trans*-synaptic transport along the axons.[84]

In AAV-mediated gene therapy with direct injection into the brain, the exogenous gene transduction of ependymal cells maintains a continuous source of transgenic products to achieve a long-term sustainable supply of exogenous proteins within the CSF.[107] In the previous studies, ependymal cells transduction was observed in the brain following ICM administration of AAV1 to non-human primate model—and ICV administration of AAV4 to PGRN-deficient mice, but not of AAVhu68 (a variant of AAV9) to NHPs.[55] In the present study, we observed efficient transduction of the ventricle and spinal ependymal cells in both AAV1- and AAV9-infected *Tmem106b*$^{-/-}$*Grn*$^{-/-}$ mice (Figures 3E and S1A). Interestingly, we have observed high PGRN levels in the serum in mice receiving AAV9- but not AAV1-*GRN* injections (Figure 3C). In the literature, it has been reported that AAV9 delivered via ICV can cross blood brain barrier,[108] resulting in AAV9 accumulation in the liver. On the other hand, AAV1 has been shown to lack the ability to cross the

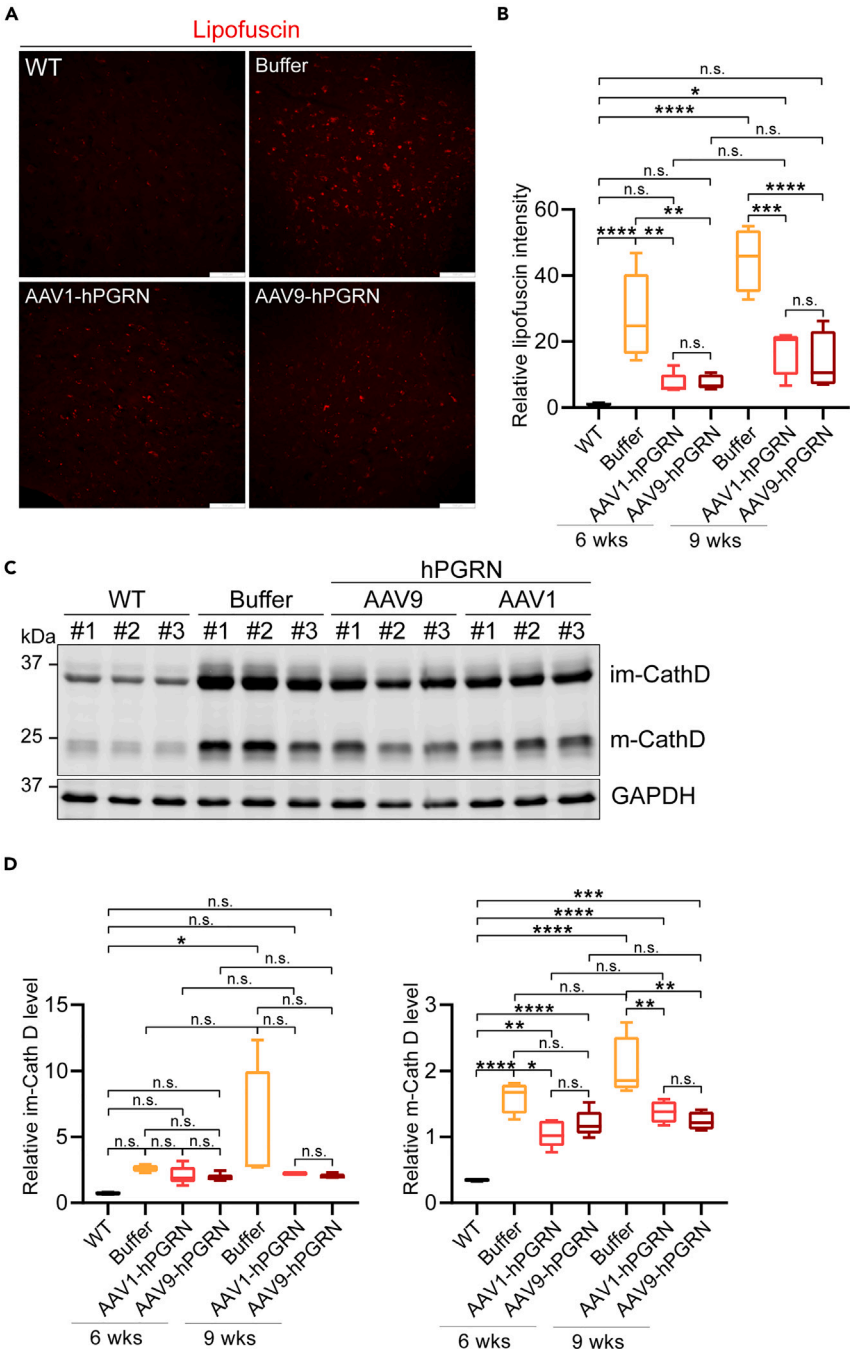

Figure 7. AAV1/9-mediated PGRN expression partially rescues the lysosome defects in the spinal cord of *Tmem106b*$^{-/-}$*Grn*$^{-/-}$ mice

(A and B) Representative fluorescence images of lipofuscin accumulation in the spinal cord sections (C1-C4) of 5-month-old WT or *Tmem106b*$^{-/-}$*Grn*$^{-/-}$ mice injected with buffer control or AAV1/9-*GRN* viruses at 6 weeks of age. The intensity of autofluorescent puncta per section was quantified. n = 4–6. Data are presented as mean ± SEM. One-way ANOVA tests with Tukey's multiple comparisons: *, $p < 0.05$, **, $p < 0.01$, ***, $p < 0.001$, ****, $p < 0.0001$; ns, no significance. Scale bar: 100 μm.

(C and D) Western blot analysis of protein levels of lysosomal enzyme cathepsin D (Cath D) and GAPDH in RIPA-soluble fractions of the spinal cord (C5-C7) from 5-month-old WT or*Tmem106b*$^{-/-}$*Grn*$^{-/-}$ mice injected with buffer control, AAV1-*GRN* or AAV9-*GRN* at 6 weeks of age. n = 4–5. Data are presented as mean ± SEM. One-way ANOVA tests with Tukey's multiple comparisons: *, $p < 0.05$, **, $p < 0.01$***, $p < 0.001$, ****, $p < 0.0001$; ns, no significance.

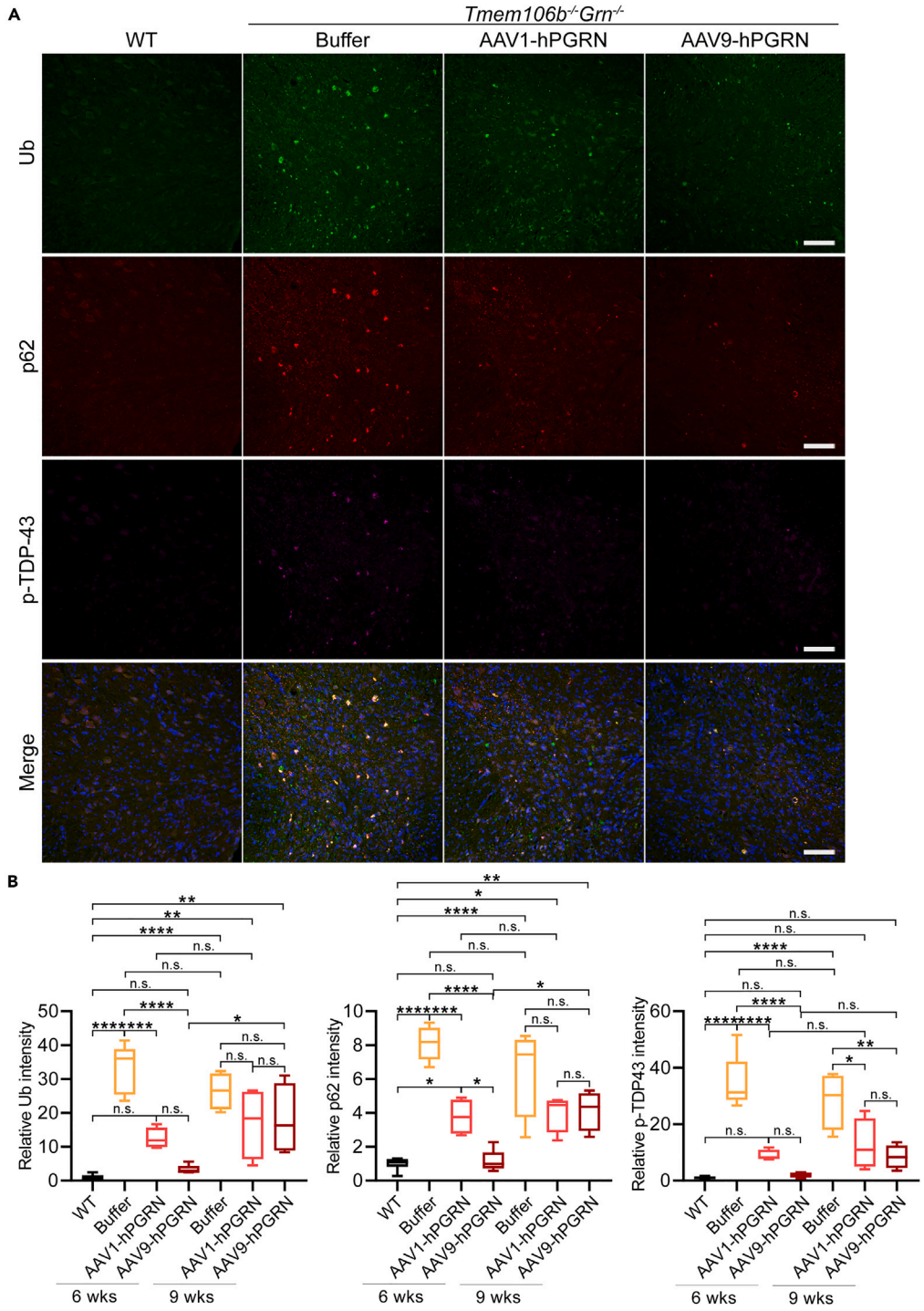

Figure 8. AAV1/9-mediated PGRN expression partially rescues ALS/FTLD-related pathology in the spinal cord of *Tmem106b*$^{-/-}$ *Grn*$^{-/-}$ mice

(A and B) Spinal cord sections (C1-C4) from 5-month-old WT or *Tmem106b*$^{-/-}$ *Grn*$^{-/-}$ mice injected with buffer control or AAV1/9-*GRN* viruses at 6 weeks of age were stained with Ub, p62, and p-TDP-43 S409/S410 antibodies (A), and the intensity of Ub, p62, or p-TDP-43 S409/S410 were quantified (B). n = 4–6. Data are presented as mean ± SEM. One-way ANOVA tests with Tukey's multiple comparisons: *, $p < 0.05$, **, $p < 0.01$, ***, $p < 0.001$, ****, $p < 0.0001$; ns, no significance. Scale bar: 100 μm.

blood brain barrier,[107,109] which is consistent with our observation that AAV1-*GRN* ICV injection does not lead to PGRN accumulation in the serum.

Limitations of the study

While our study demonstrates that *Tmem106b*$^{-/-}$*Grn*$^{-/-}$ mouse strain is a robust mouse model to test the efficacy of AAV-*GRN* constructs at pathological and behavioral levels, there are several limitations. First of all, this mouse model cannot be used to test the effect of molecules enhancing PGRN expression or function, since PGRN is completely ablated in this mouse model instead of being haploinsufficient as in human FTLD-*GRN* patients. Secondly, since the strongest phenotype we have observed in *Tmem106b*$^{-/-}$*Grn*$^{-/-}$ mice are in the spinal cord rather than in the brain, the rescue effect of AAV-*GRN* constructs was hard to assess in the brain. Thirdly, due to insufficient CSF samples, we could not compare PGRN levels in the serum versus CSF in AAV9-*GRN* injected mice. Finally, viruses could be injected at different times to determine the efficacy of AAV-*GRN* in preventing versus rescuing motor deficits and ALS/FTD related pathologies.

STAR★METHODS

Detailed methods are provided in the online version of this paper and include the following:

- KEY RESOURCES TABLE
- RESOURCE AVAILABILITY
  - Lead contact
  - Materials availability
  - Data and code availability
- EXPERIMENTAL MODEL AND STUDY PARTICIPANT DETAILS
  - Mouse strains
  - AAV plasmids, capsids, and testing
- METHOD DETAILS
  - Stereotactic injection of AAV
  - Behavioral test
  - Tissue preparation for western blot analysis
  - Human PGRN ELISA
  - Immunofluorescence staining
  - Image acquisition and analysis
- QUANTIFICATION AND STATISTICAL ANALYSIS

SUPPLEMENTAL INFORMATION

Supplemental information can be found online at https://doi.org/10.1016/j.isci.2023.107247.

ACKNOWLEDGMENTS

We would like to thank Xiaochun Wu for technical assistance, Dr. Tony Bretscher's lab for assistance with the confocal microscope, and Dr. Chris Schaffer and Dr. Nozomi Nishimura's lab for assistance with behavioral tests. This work is funded by Alector and funding to F. H from NIA and NINDS (R01NS095954 and R01NS088448).

AUTHOR CONTRIBUTIONS

T.F. bred the mice, performed the ICV injection, characterized all the behavorial and pathological phenotypes and anlaysed the results with the help from P.L. and H.X.Q. G.M. designed the plasmids, selected capsids and managed the manufacturing process and testing of plasmids and AAV in cells. G.W., A.K., J.P. and K.P. performed testing of plasmids and AAV analysis. F.H., T.F., M.K., G.M., N.A.D, A.M., and H.L. designed the study, anlaysed the results, and supervised the project. F.H. wrote the manuscript together with T.F.

DECLARATION OF INTERESTS

The authors T.F., P.L., H.X.Q., and F.H. declare that they have no conflict of interest. M.K., A.M., G.M., G.W. J.P., K.P., A.K., H.L., and N.D. are/were employees of Alector and may have an equity interest in Alector, Inc.

Received: March 22, 2023
Revised: May 18, 2023
Accepted: June 26, 2023
Published: June 28, 2023

REFERENCES

1. Baker, M., Mackenzie, I.R., Pickering-Brown, S.M., Gass, J., Rademakers, R., Lindholm, C., Snowden, J., Adamson, J., Sadovnick, A.D., Rollinson, S., et al. (2006). Mutations in progranulin cause tau-negative frontotemporal dementia linked to chromosome 17. Nature *442*, 916–919.

2. Cruts, M., Gijselinck, I., van der Zee, J., Engelborghs, S., Wils, H., Pirici, D., Rademakers, R., Vandenberghe, R., Dermaut, B., Martin, J.J., et al. (2006). Null mutations in progranulin cause ubiquitin-positive frontotemporal dementia linked to chromosome 17q21. Nature *442*, 920–924.

3. Gass, J., Cannon, A., Mackenzie, I.R., Boeve, B., Baker, M., Adamson, J., Crook, R., Melquist, S., Kuntz, K., Petersen, R., et al. (2006). Mutations in progranulin are a major cause of ubiquitin-positive frontotemporal lobar degeneration. Hum. Mol. Genet. *15*, 2988–3001.

4. Almeida, M.R., Macario, M.C., Ramos, L., Baldeiras, I., Ribeiro, M.H., and Santana, I. (2016). Portuguese family with the co-occurrence of frontotemporal lobar degeneration and neuronal ceroid lipofuscinosis phenotypes due to progranulin gene mutation. Neurobiol. Aging *41*, 200.e1–200.e5. https://doi.org/10.1016/j.neurobiolaging.2016.02.019.

5. Smith, K.R., Damiano, J., Franceschetti, S., Carpenter, S., Canafoglia, L., Morbin, M., Rossi, G., Pareyson, D., Mole, S.E., Staropoli, J.F., et al. (2012). Strikingly different clinicopathological phenotypes determined by progranulin-mutation dosage. Am. J. Hum. Genet. *90*, 1102–1107. https://doi.org/10.1016/j.ajhg.2012.04.021 S0002-9297(12)00254-6.

6. Canafoglia, L., Morbin, M., Scaioli, V., Pareyson, D., D'Incerti, L., Fugnanesi, V., Tagliavini, F., Berkovic, S.F., and Franceschetti, S. (2014). Recurrent generalized seizures, visual loss, and palinopsia as phenotypic features of neuronal ceroid lipofuscinosis due to progranulin gene mutation. Epilepsia *55*, e56–e59. https://doi.org/10.1111/epi.12632.

7. Bellenguez, C., Grenier-Boley, B., and Lambert, J.C. (2020). Genetics of Alzheimer's disease: where we are, and where we are going. Curr. Opin. Neurobiol. *61*, 40–48. https://doi.org/10.1016/j.conb.2019.11.024.

8. Nelson, P.T., Dickson, D.W., Trojanowski, J.Q., Jack, C.R., Boyle, P.A., Arfanakis, K., Rademakers, R., Alafuzoff, I., Attems, J., Brayne, C., et al. (2019). Limbic-predominant age-related TDP-43 encephalopathy (LATE): consensus working group report. Brain *142*, 1503–1527. https://doi.org/10.1093/brain/awz099.

9. van Blitterswijk, M., Mullen, B., Wojtas, A., Heckman, M.G., Diehl, N.N., Baker, M.C., DeJesus-Hernandez, M., Brown, P.H., Murray, M.E., Hsiung, G.Y.R., et al. (2014). Genetic modifiers in carriers of repeat expansions in the C9ORF72 gene. Mol. Neurodegener. *9*, 38. https://doi.org/10.1186/1750-1326-9-38.

10. Nalls, M.A., Blauwendraat, C., Vallerga, C.L., Heilbron, K., Bandres-Ciga, S., Chang, D., Tan, M., Kia, D.A., Noyce, A.J., Xue, A., et al. (2019). Identification of novel risk loci, causal insights, and heritable risk for Parkinson's disease: a meta-analysis of genome-wide association studies. Lancet Neurol. *18*, 1091–1102. https://doi.org/10.1016/S1474-4422(19)30320-5.

11. Jian, J., Zhao, S., Tian, Q.Y., Liu, H., Zhao, Y., Chen, W.C., Grunig, G., Torres, P.A., Wang, B.C., Zeng, B., et al. (2016). Association Between Progranulin and Gaucher Disease. EBioMedicine *11*, 127–137. https://doi.org/10.1016/j.ebiom.2016.08.004.

12. Rhinn, H., Tatton, N., McCaughey, S., Kurnellas, M., and Rosenthal, A. (2022). Progranulin as a therapeutic target in neurodegenerative diseases. Trends Pharmacol. Sci. *43*, 641–652. https://doi.org/10.1016/j.tips.2021.11.015.

13. Bateman, A., and Bennett, H.P.J. (2009). The granulin gene family: from cancer to dementia. Bioessays *31*, 1245–1254. https://doi.org/10.1002/bies.200900086.

14. Beel, S., Moisse, M., Damme, M., De Muynck, L., Robberecht, W., Van Den Bosch, L., Saftig, P., and Van Damme, P. (2017). Progranulin functions as a cathepsin D chaperone to stimulate axonal outgrowth in vivo. Hum. Mol. Genet. *26*, 2850–2863.

15. Kleinberger, G., Capell, A., Haass, C., and Van Broeckhoven, C. (2013). Mechanisms of granulin deficiency: lessons from cellular and animal models. Mol. Neurobiol. *47*, 337–360. https://doi.org/10.1007/s12035-012-8380-8.

16. Gass, J., Lee, W.C., Cook, C., Finch, N., Stetler, C., Jansen-West, K., Lewis, J., Link, C.D., Rademakers, R., Nykjær, A., and Petrucelli, L. (2012). Progranulin regulates neuronal outgrowth independent of sortilin. Mol. Neurodegener. *7*, 33. https://doi.org/10.1186/1750-1326-7-33.

17. Gao, X., Joselin, A.P., Wang, L., Kar, A., Ray, P., Bateman, A., Goate, A.M., and Wu, J.Y. (2010). Progranulin promotes neurite outgrowth and neuronal differentiation by regulating GSK-3beta. Protein Cell *1*, 552–562. https://doi.org/10.1007/s13238-010-0067-1.

18. Van Damme, P., Van Hoecke, A., Lambrechts, D., Vanacker, P., Bogaert, E., van Swieten, J., Carmeliet, P., Van Den Bosch, L., and Robberecht, W. (2008). Progranulin functions as a neurotrophic factor to regulate neurite outgrowth and enhance neuronal survival. J. Cell Biol. *181*, 37–41. https://doi.org/10.1083/jcb.200712039.

19. Toh, H., Chitramuthu, B.P., Bennett, H.P.J., and Bateman, A. (2011). Structure, function, and mechanism of progranulin; the brain and beyond. J. Mol. Neurosci. *45*, 538–548. https://doi.org/10.1007/s12031-011-9569-4.

20. Cenik, B., Sephton, C.F., Kutluk Cenik, B., Herz, J., and Yu, G. (2012). Progranulin: a proteolytically processed protein at the crossroads of inflammation and neurodegeneration. J. Biol. Chem. *287*, 32298–32306. https://doi.org/10.1074/jbc.R112.399170.

21. Tanaka, Y., Matsuwaki, T., Yamanouchi, K., and Nishihara, M. (2013). Exacerbated inflammatory responses related to activated microglia after traumatic brain injury in progranulin-deficient mice. Neuroscience *231*, 49–60. https://doi.org/10.1016/j.neuroscience.2012.11.032.

22. Kao, A.W., McKay, A., Singh, P.P., Brunet, A., and Huang, E.J. (2017). Progranulin, lysosomal regulation and neurodegenerative disease. Nat. Rev. Neurosci. *18*, 325–333. https://doi.org/10.1038/nrn.2017.36.

23. Lui, H., Zhang, J., Makinson, S.R., Cahill, M.K., Kelley, K.W., Huang, H.Y., Shang, Y., Oldham, M.C., Martens, L.H., Gao, F., et al. (2016). Progranulin Deficiency Promotes Circuit-Specific Synaptic Pruning by Microglia via Complement Activation. Cell *165*, 921–935. https://doi.org/10.1016/j.cell.2016.04.001.

24. Pickford, F., Marcus, J., Camargo, L.M., Xiao, Q., Graham, D., Mo, J.R., Burkhardt, M., Kulkarni, V., Crispino, J., Hering, H., and Hutton, M. (2011). Progranulin is a chemoattractant for microglia and stimulates their endocytic activity. Am. J. Pathol. *178*, 284–295. https://doi.org/10.1016/j.ajpath.2010.11.002.

25. Yin, F., Banerjee, R., Thomas, B., Zhou, P., Qian, L., Jia, T., Ma, X., Ma, Y., Iadecola, C., Beal, M.F., et al. (2010). Exaggerated inflammation, impaired host defense, and neuropathology in progranulin-deficient mice. J. Exp. Med. *207*, 117–128. https://doi.org/10.1084/jem.20091568.

26. Paushter, D.H., Du, H., Feng, T., and Hu, F. (2018). The lysosomal function of progranulin, a guardian against neurodegeneration. Acta Neuropathol. *136*, 1–17. https://doi.org/10.1007/s00401-018-1861-8.

27. Zhou, X., Kukar, T., and Rademakers, R. (2021). Lysosomal Dysfunction and Other Pathomechanisms in FTLD: Evidence from Progranulin Genetics and Biology. Adv. Exp. Med. Biol. *1281*, 219–242. https://doi.org/10.1007/978-3-030-51140-1_14.

28. Hu, F., Padukkavidana, T., Vægter, C.B., Brady, O.A., Zheng, Y., Mackenzie, I.R., Feldman, H.H., Nykjaer, A., and Strittmatter, S.M. (2010). Sortilin-mediated endocytosis determines levels of the frontotemporal dementia protein, progranulin. Neuron *68*, 654–667. https://doi.org/10.1016/j.neuron.2010.09.034.

29. Zhou, X., Sun, L., Bastos de Oliveira, F., Qi, X., Brown, W.J., Smolka, M.B., Sun, Y., and Hu, F. (2015). Prosaposin facilitates sortilin-independent lysosomal trafficking of progranulin. J. Cell Biol. *210*, 991–1002. https://doi.org/10.1083/jcb.201502029.

30. Zhou, X., Sun, L., Bracko, O., Choi, J.W., Jia, Y., Nana, A.L., Brady, O.A., Hernandez, J.C.C., Nishimura, N., Seeley, W.W., and Hu, F. (2017). Impaired prosaposin lysosomal trafficking in frontotemporal lobar degeneration due to progranulin mutations. Nat. Commun. *8*, 15277. https://doi.org/10.1038/ncomms15277.

31. Holler, C.J., Taylor, G., Deng, Q., and Kukar, T. (2017). Intracellular Proteolysis of Progranulin Generates Stable, Lysosomal Granulins that Are Haploinsufficient in Patients with Frontotemporal Dementia Caused by GRN Mutations. eNeuro *4*. https://doi.org/10.1523/ENEURO.0100-17.2017.

32. Lee, C.W., Stankowski, J.N., Chew, J., Cook, C.N., Lam, Y.W., Almeida, S., Carlomagno, Y., Lau, K.F., Prudencio, M., Gao, F.B., et al. (2017). The lysosomal protein cathepsin L is a progranulin protease. Mol. Neurodegener. *12*, 55. https://doi.org/10.1186/s13024-017-0196-6.

33. Zhou, X., Paushter, D.H., Feng, T., Sun, L., Reinheckel, T., and Hu, F. (2017). Lysosomal processing of progranulin. Mol. Neurodegener. *12*, 62. https://doi.org/10.1186/s13024-017-0205-9.

34. Belcastro, V., Siciliano, V., Gregoretti, F., Mithbaokar, P., Dharmalingam, G., Berlingieri, S., Iorio, F., Oliva, G., Polishchuck, R., Brunetti-Pierri, N., and di Bernardo, D. (2011). Transcriptional gene network inference from a massive dataset elucidates transcriptome organization and gene function. Nucleic Acids Res. *39*, 8677–8688. https://doi.org/10.1093/nar/gkr593.

35. Sardiello, M., Palmieri, M., di Ronza, A., Medina, D.L., Valenza, M., Gennarino, V.A., Di Malta, C., Donaudy, F., Embrione, V., Polishchuk, R.S., et al. (2009). A gene network regulating lysosomal biogenesis and function. Science *325*, 473–477. https://doi.org/10.1126/science.1174447.

36. Tanaka, Y., Matsuwaki, T., Yamanouchi, K., and Nishihara, M. (2013). Increased lysosomal biogenesis in activated microglia and exacerbated neuronal damage after traumatic brain injury in progranulin-deficient mice. Neuroscience *250*, 8–19. https://doi.org/10.1016/j.neuroscience.2013.06.049.

37. Ahmed, Z., Sheng, H., Xu, Y.F., Lin, W.L., Innes, A.E., Gass, J., Yu, X., Wuertzer, C.A., Hou, H., Chiba, S., et al. (2010). Accelerated lipofuscinosis and ubiquitination in granulin knockout mice suggest a role for progranulin in successful aging. Am. J. Pathol. *177*, 311–324. https://doi.org/10.2353/ajpath.2010.090915.

38. Tanaka, Y., Chambers, J.K., Matsuwaki, T., Yamanouchi, K., and Nishihara, M. (2014). Possible involvement of lysosomal dysfunction in pathological changes of the brain in aged progranulin-deficient mice. Acta Neuropathol. Commun. *2*, 78. https://doi.org/10.1186/s40478-014-0078-x s40478-014-0078-x.

39. Götzl, J.K., Mori, K., Damme, M., Fellerer, K., Tahirovic, S., Kleinberger, G., Janssens, J., van der Zee, J., Lang, C.M., Kremmer, E., et al. (2014). Common pathobiochemical hallmarks of progranulin-associated frontotemporal lobar degeneration and neuronal ceroid lipofuscinosis. Acta Neuropathol. *127*, 845–860. https://doi.org/10.1007/s00401-014-1262-6.

40. Ward, M.E., Chen, R., Huang, H.Y., Ludwig, C., Telpoukhovskaia, M., Taubes, A., Boudin, H., Minami, S.S., Reichert, M., Albrecht, P., et al. (2017). Individuals with progranulin haploinsufficiency exhibit features of neuronal ceroid lipofuscinosis. Sci. Transl. Med. *9*, eaah5642. https://doi.org/10.1126/scitranslmed.aah5642.

41. Zhou, X., Paushter, D.H., Feng, T., Pardon, C.M., Mendoza, C.S., and Hu, F. (2017). Regulation of cathepsin D activity by the FTLD protein progranulin. Acta Neuropathol. *134*, 151–153. https://doi.org/10.1007/s00401-017-1719-5.

42. Valdez, C., Wong, Y.C., Schwake, M., Bu, G., Wszolek, Z.K., and Krainc, D. (2017). Progranulin-mediated deficiency of cathepsin D results in FTD and NCL-like phenotypes in neurons derived from FTD patients. Hum. Mol. Genet. *26*, 4861–4872. https://doi.org/10.1093/hmg/ddx364.

43. Butler, V.J., Cortopassi, W.A., Argouarch, A.R., Ivry, S.L., Craik, C.S., Jacobson, M.P., and Kao, A.W. (2019). Progranulin Stimulates the In Vitro Maturation of Pro-Cathepsin D at Acidic pH. J. Mol. Biol. *431*, 1038–1047. https://doi.org/10.1016/j.jmb.2019.01.027.

44. Arrant, A.E., Roth, J.R., Boyle, N.R., Kashyap, S.N., Hoffmann, M.Q., Murchison, C.F., Ramos, E.M., Nana, A.L., Spina, S., Grinberg, L.T., et al. (2019). Impaired beta-glucocerebrosidase activity and processing in frontotemporal dementia due to progranulin mutations. Acta Neuropathol. Commun. *7*, 218. https://doi.org/10.1186/s40478-019-0872-6.

45. Valdez, C., Ysselstein, D., Young, T.J., Zheng, J., and Krainc, D. (2020). Progranulin mutations result in impaired processing of prosaposin and reduced glucocerebrosidase activity. Hum. Mol. Genet. *29*, 716–726. https://doi.org/10.1093/hmg/ddz229.

46. Zhou, X., Paushter, D.H., Pagan, M.D., Kim, D., Nunez Santos, M., Lieberman, R.L., Overkleeft, H.S., Sun, Y., Smolka, M.B., and Hu, F. (2019). Progranulin deficiency leads to reduced glucocerebrosidase activity. PLoS One *14*, e0212382. https://doi.org/10.1371/journal.pone.0212382.

47. Boland, S., Swarup, S., Ambaw, Y.A., Malia, P.C., Richards, R.C., Fischer, A.W., Singh, S., Aggarwal, G., Spina, S., Nana, A.L., et al. (2022). Deficiency of the frontotemporal dementia gene GRN results in gangliosidosis. Nat. Commun. *13*, 5924. https://doi.org/10.1038/s41467-022-33500-9.

48. Logan, T., Simon, M.J., Rana, A., Cherf, G.M., Srivastava, A., Davis, S.S., Low, R.L.Y., Chiu, C.L., Fang, M., Huang, F., et al. (2021). Rescue of a lysosomal storage disorder caused by Grn loss of function with a brain penetrant progranulin biologic. Cell *184*, 4651–4668.e25. https://doi.org/10.1016/j.cell.2021.08.002.

49. Showalter, M.R., Berg, A.L., Nagourney, A., Heil, H., Carraway, K.L., 3rd, and Fiehn, O. (2020). The Emerging and Diverse Roles of Bis(monoacylglycero) Phosphate Lipids in Cellular Physiology and Disease. Int. J. Mol. Sci. *21*, 8067. https://doi.org/10.3390/ijms21218067.

50. Amin, S., Carling, G., and Gan, L. (2022). New insights and therapeutic opportunities for progranulin-deficient frontotemporal dementia. Curr. Opin. Neurobiol. *72*, 131–139. https://doi.org/10.1016/j.conb.2021.10.001.

51. Simon, M.J., Logan, T., DeVos, S.L., and Di Paolo, G. (2023). Lysosomal functions of progranulin and implications for treatment of frontotemporal dementia. Trends Cell Biol. *33*, 324–339. https://doi.org/10.1016/j.tcb.2022.09.006.

52. Riyad, J.M., and Weber, T. (2021). Intracellular trafficking of adeno-associated virus (AAV) vectors: challenges and future directions. Gene Ther. *28*, 683–696. https://doi.org/10.1038/s41434-021-00243-z.

53. Arrant, A.E., Filiano, A.J., Unger, D.E., Young, A.H., and Roberson, E.D. (2017). Restoring neuronal progranulin reverses deficits in a mouse model of frontotemporal dementia. Brain *140*, 1447–1465. https://doi.org/10.1093/brain/awx060.

54. Arrant, A.E., Onyilo, V.C., Unger, D.E., and Roberson, E.D. (2018). Progranulin Gene Therapy Improves Lysosomal Dysfunction and Microglial Pathology Associated with Frontotemporal Dementia and Neuronal Ceroid Lipofuscinosis. J. Neurosci. *38*, 2341–2358. https://doi.org/10.1523/JNEUROSCI.3081-17.2018.

55. Hinderer, C., Miller, R., Dyer, C., Johansson, J., Bell, P., Buza, E., and Wilson, J.M. (2020). Adeno-associated virus serotype 1-based gene therapy for FTD caused by GRN mutations. Ann. Clin. Transl. Neurol. *7*, 1843–1853. https://doi.org/10.1002/acn3.51165.

56. Ertl, H.C.J. (2021). T Cell-Mediated Immune Responses to AAV and AAV Vectors. Front. Immunol. *12*, 666666. https://doi.org/10.3389/fimmu.2021.666666.

57. Mays, L.E., and Wilson, J.M. (2011). The complex and evolving story of T cell activation to AAV vector-encoded transgene products. Mol. Ther. *19*, 16–27. https://doi.org/10.1038/mt.2010.250.

58. Amado, D.A., Rieders, J.M., Diatta, F., Hernandez-Con, P., Singer, A., Mak, J.T., Zhang, J., Lancaster, E., Davidson, B.L., and Chen-Plotkin, A.S. (2019). AAV-Mediated Progranulin Delivery to a Mouse Model of Progranulin Deficiency Causes T Cell-Mediated Toxicity. Mol. Ther. *27*, 465–478. https://doi.org/10.1016/j.ymthe.2018.11.013.

59. Cruchaga, C., Graff, C., Chiang, H.H., Wang, J., Hinrichs, A.L., Spiegel, N., Bertelsen, S., Mayo, K., Norton, J.B., Morris, J.C., and Goate, A. (2011). Association of TMEM106B gene polymorphism with age at onset in granulin mutation carriers and plasma granulin protein levels. Arch. Neurol. *68*, 581–586. https://doi.org/10.1001/archneurol.2010.350.

60. Finch, N., Carrasquillo, M.M., Baker, M., Rutherford, N.J., Coppola, G., Dejesus-Hernandez, M., Crook, R., Hunter, T., Ghidoni, R., Benussi, L., et al. (2011). TMEM106B regulates progranulin levels and the penetrance of FTLD in GRN mutation carriers. Neurology *76*, 467–474. https://doi.org/10.1212/WNL.0b013e31820a0e3b.

61. Van Deerlin, V.M., Sleiman, P.M.A., Martinez-Lage, M., Chen-Plotkin, A., Wang, L.S., Graff-Radford, N.R., Dickson, D.W., Rademakers, R., Boeve, B.F., Grossman, M., et al. (2010). Common variants at 7p21 are associated with frontotemporal lobar degeneration with TDP-43 inclusions. Nat. Genet. *42*, 234–239. https://doi.org/10.1038/ng.536.

62. van der Zee, J., Van Langenhove, T., Kleinberger, G., Sleegers, K., Engelborghs, S., Vandenberghe, R., Santens, P., Van den Broeck, M., Joris, G., Brys, J., et al. (2011). TMEM106B is associated with frontotemporal lobar degeneration in a clinically diagnosed patient cohort. Brain *134*, 808–815. https://doi.org/10.1093/brain/awr007.

63. van Blitterswijk, M., Mullen, B., Nicholson, A.M., Bieniek, K.F., Heckman, M.G., Baker, M.C., DeJesus-Hernandez, M., Finch, N.A., Brown, P.H., Murray, M.E., et al. (2014). TMEM106B protects C9ORF72 expansion carriers against frontotemporal dementia. Acta Neuropathol. *127*, 397–406. https://doi.org/10.1007/s00401-013-1240-4.

64. Brady, O.A., Zheng, Y., Murphy, K., Huang, M., and Hu, F. (2013). The frontotemporal lobar degeneration risk factor, TMEM106B, regulates lysosomal morphology and function. Hum. Mol. Genet. *22*, 685–695. https://doi.org/10.1093/hmg/dds475.

65. Chen-Plotkin, A.S., Unger, T.L., Gallagher, M.D., Bill, E., Kwong, L.K., Volpicelli-Daley, L., Busch, J.I., Akle, S., Grossman, M., Van Deerlin, V., et al. (2012). TMEM106B, the risk gene for frontotemporal dementia, is regulated by the microRNA-132/212 cluster and affects progranulin pathways. J. Neurosci. *32*, 11213–11227. https://doi.org/10.1523/JNEUROSCI.0521-12.2012.

66. Lang, C.M., Fellerer, K., Schwenk, B.M., Kuhn, P.H., Kremmer, E., Edbauer, D., Capell, A., and Haass, C. (2012). Membrane orientation and subcellular localization of transmembrane protein 106B (TMEM106B), a major risk factor for frontotemporal lobar degeneration. J. Biol. Chem. *287*, 19355–19365. https://doi.org/10.1074/jbc.M112.365098.

67. Stagi, M., Klein, Z.A., Gould, T.J., Bewersdorf, J., and Strittmatter, S.M. (2014). Lysosome size, motility and stress response regulated by fronto-temporal dementia modifier TMEM106B. Mol. Cell. Neurosci. *61*, 226–240. https://doi.org/10.1016/j.mcn.2014.07.006.

68. Klein, Z.A., Takahashi, H., Ma, M., Stagi, M., Zhou, M., Lam, T.T., and Strittmatter, S.M. (2017). Loss of TMEM106B Ameliorates Lysosomal and Frontotemporal Dementia-Related Phenotypes in Progranulin-Deficient Mice. Neuron *95*, 281–296.e6. https://doi.org/10.1016/j.neuron.2017.06.026.

69. Kundu, S.T., Grzeskowiak, C.L., Fradette, J.J., Gibson, L.A., Rodriguez, L.B., Creighton, C.J., Scott, K.L., and Gibbons, D.L. (2018). TMEM106B drives lung cancer metastasis by inducing TFEB-dependent lysosome synthesis and secretion of cathepsins. Nat. Commun. *9*, 2731. https://doi.org/10.1038/s41467-018-05013-x.

70. Zhang, T., Pang, W., Feng, T., Guo, J., Wu, K., Nunez Santos, M., Arthanarisami, A., Nana, A.L., Nguyen, Q., Kim, P.J., et al. (2023). TMEM106B regulates microglial proliferation and survival in response to demyelination. Sci. Adv. *9*, eadd2676. https://doi.org/10.1126/sciadv.add2676.

71. Feng, T., Sheng, R.R., Solé-Domènech, S., Ullah, M., Zhou, X., Mendoza, C.S., Enriquez, L.C.M., Katz, I.I., Paushter, D.H., Sullivan, P.M., et al. (2020). A role of the frontotemporal lobar degeneration risk factor TMEM106B in myelination. Brain *143*, 2255–2271. https://doi.org/10.1093/brain/awaa154.

72. Schwenk, B.M., Lang, C.M., Hogl, S., Tahirovic, S., Orozco, D., Rentzsch, K., Lichtenthaler, S.F., Hoogenraad, C.C., Capell, A., Haass, C., and Edbauer, D. (2014). The FTLD risk factor TMEM106B and MAP6 control dendritic trafficking of lysosomes. EMBO J. *33*, 450–467. https://doi.org/10.1002/embj.201385857.

73. Feng, T., Mai, S., Roscoe, J.M., Sheng, R.R., Ullah, M., Zhang, J., Katz, I.I., Yu, H., Xiong, W., and Hu, F. (2020). Loss of TMEM106B and PGRN leads to severe lysosomal abnormalities and neurodegeneration in mice. EMBO Rep. *21*, e50219. https://doi.org/10.15252/embr.202050219.

74. Luningschror, P., Werner, G., Stroobants, S., Kakuta, S., Dombert, B., Sinske, D., Wanner, R., Lullmann-Rauch, R., Wefers, B., Wurst, W., et al. (2020). The FTLD Risk Factor TMEM106B Regulates the Transport of Lysosomes at the Axon Initial Segment of Motoneurons. Cell Rep. *30*, 3506–3519.e3506. https://doi.org/10.1016/j.celrep.2020.02.060.

75. Zhou, X., Nicholson, A.M., Ren, Y., Brooks, M., Jiang, P., Zuberi, A., Phuoc, H.N., Perkerson, R.B., Matchett, B., Parsons, T.M., et al. (2020). Loss of TMEM106B leads to myelination deficits: implications for frontotemporal dementia treatment strategies. Brain *143*, 1905–1919. https://doi.org/10.1093/brain/awaa141.

76. Stroobants, S., D'Hooge, R., and Damme, M. (2021). Aged Tmem106b knockout mice display gait deficits in coincidence with Purkinje cell loss and only limited signs of non-motor dysfunction. Brain Pathol. *31*, 223–238. https://doi.org/10.1111/bpa.12903.

77. Rademakers, R., Nicholson, A.M., Ren, Y., Koga, S., Nguyen, H.P., Brooks, M., Qiao, W., Quicksall, Z.S., Matchett, B., Perkerson, R.B., et al. (2021). Loss of Tmem106b leads to cerebellum Purkinje cell death and motor deficits. Brain Pathol. *31*, e12945. https://doi.org/10.1111/bpa.12945.

78. Feng, T., Luan, L., Katz, I.I., Ullah, M., Van Deerlin, V.M., Trojanowski, J.Q., Lee, E.B., and Hu, F. (2022). TMEM106B deficiency impairs cerebellar myelination and synaptic integrity with Purkinje cell loss. Acta Neuropathol. Commun. *10*, 33. https://doi.org/10.1186/s40478-022-01334-7.

79. Feng, T., Lacrampe, A., and Hu, F. (2021). Physiological and pathological functions of TMEM106B: a gene associated with brain aging and multiple brain disorders. Acta Neuropathol. *141*, 327–339. https://doi.org/10.1007/s00401-020-02246-3.

80. Zhou, X., Brooks, M., Jiang, P., Koga, S., Zuberi, A.R., Baker, M.C., Parsons, T.M., Castanedes-Casey, M., Phillips, V., Librero, A.L., et al. (2020). Loss of Tmem106b exacerbates FTLD pathologies and causes motor deficits in progranulin-deficient mice. EMBO Rep. *21*, e50197. https://doi.org/10.15252/embr.202050197.

81. Werner, G., Damme, M., Schludi, M., Gnörich, J., Wind, K., Fellerer, K., Wefers, B., Wurst, W., Edbauer, D., Brendel, M., et al. (2020). Loss of TMEM106B potentiates lysosomal and FTLD-like pathology in progranulin-deficient mice. EMBO Rep. *21*, e50241. https://doi.org/10.15252/embr.202050241.

82. Lunev, E., Karan, A., Egorova, T., and Bardina, M. (2022). Adeno-Associated Viruses for Modeling Neurological Diseases

in Animals: Achievements and Prospects. Biomedicines *10*, 1140. https://doi.org/10.3390/biomedicines10051140.

83. Bulcha, J.T., Wang, Y., Ma, H., Tai, P.W.L., and Gao, G. (2021). Viral vector platforms within the gene therapy landscape. Signal Transduct. Targeted Ther. *6*, 53. https://doi.org/10.1038/s41392-021-00487-6.

84. Haery, L., Deverman, B.E., Matho, K.S., Cetin, A., Woodard, K., Cepko, C., Guerin, K.I., Rego, M.A., Ersing, I., Bachle, S.M., et al. (2019). Adeno-Associated Virus Technologies and Methods for Targeted Neuronal Manipulation. Front. Neuroanat. *13*, 93. https://doi.org/10.3389/fnana.2019.00093.

85. Choudhury, S.R., Hudry, E., Maguire, C.A., Sena-Esteves, M., Breakefield, X.O., and Grandi, P. (2017). Viral vectors for therapy of neurologic diseases. Neuropharmacology *120*, 63–80. https://doi.org/10.1016/j.neuropharm.2016.02.013.

86. Du, H., Zhou, X., Feng, T., and Hu, F. (2022). Regulation of lysosomal trafficking of progranulin by sortilin and prosaposin. Brain Commun. *4*, fcab310. https://doi.org/10.1093/braincomms/fcab310.

87. Lalonde, R., and Strazielle, C. (2011). Brain regions and genes affecting limb-clasping responses. Brain Res. Rev. *67*, 252–259. https://doi.org/10.1016/j.brainresrev.2011.02.005.

88. Cantoni, C., Bollman, B., Licastro, D., Xie, M., Mikesell, R., Schmidt, R., Yuede, C.M., Galimberti, D., Olivecrona, G., Klein, R.S., et al. (2015). TREM2 regulates microglial cell activation in response to demyelination in vivo. Acta Neuropathol. *129*, 429–447. https://doi.org/10.1007/s00401-015-1388-1.

89. Filiano, A.J., Martens, L.H., Young, A.H., Warmus, B.A., Zhou, P., Diaz-Ramirez, G., Jiao, J., Zhang, Z., Huang, E.J., Gao, F.B., et al. (2013). Dissociation of frontotemporal dementia-related deficits and neuroinflammation in progranulin haploinsufficient mice. J. Neurosci. *33*, 5352–5361. https://doi.org/10.1523/JNEUROSCI.6103-11.2013.

90. Gray, S.J., Foti, S.B., Schwartz, J.W., Bachaboina, L., Taylor-Blake, B., Coleman, J., Ehlers, M.D., Zylka, M.J., McCown, T.J., and Samulski, R.J. (2011). Optimizing promoters for recombinant adeno-associated virus-mediated gene expression in the peripheral and central nervous system using self-complementary vectors. Hum. Gene Ther. *22*, 1143–1153. https://doi.org/10.1089/hum.2010.245.

91. Zheng, Y., Brady, O.A., Meng, P.S., Mao, Y., and Hu, F. (2011). C-terminus of progranulin interacts with the beta-propeller region of sortilin to regulate progranulin trafficking. PLoS One *6*, e21023. https://doi.org/10.1371/journal.pone.0021023 PONE-D-11-00375.

92. Xiong, W., Wu, D.M., Xue, Y., Wang, S.K., Chung, M.J., Ji, X., Rana, P., Zhao, S.R., Mai, S., and Cepko, C.L. (2019). AAV cis-regulatory sequences are correlated with ocular toxicity. Proc. Natl. Acad. Sci. USA *116*, 5785–5794. https://doi.org/10.1073/pnas.1821000116.

93. Bailey, L.A., Hatton, D., Field, R., and Dickson, A.J. (2012). Determination of Chinese hamster ovary cell line stability and recombinant antibody expression during long-term culture. Biotechnol. Bioeng. *109*, 2093–2103. https://doi.org/10.1002/bit.24485.

94. He, L., Winterrowd, C., Kadura, I., and Frye, C. (2012). Transgene copy number distribution profiles in recombinant CHO cell lines revealed by single cell analyses. Biotechnol. Bioeng. *109*, 1713–1722. https://doi.org/10.1002/bit.24428.

95. Hsu, C.C., Li, H.P., Hung, Y.H., Leu, Y.W., Wu, W.H., Wang, F.S., Lee, K.D., Chang, P.J., Wu, C.S., Lu, Y.J., et al. (2010). Targeted methylation of CMV and E1A viral promoters. Biochem. Biophys. Res. Commun. *402*, 228–234. https://doi.org/10.1016/j.bbrc.2010.09.131.

96. Moritz, B., Becker, P.B., and Göpfert, U. (2015). CMV promoter mutants with a reduced propensity to productivity loss in CHO cells. Sci. Rep. *5*, 16952. https://doi.org/10.1038/srep16952.

97. Osterlehner, A., Simmeth, S., and Göpfert, U. (2011). Promoter methylation and transgene copy numbers predict unstable protein production in recombinant Chinese hamster ovary cell lines. Biotechnol. Bioeng. *108*, 2670–2681. https://doi.org/10.1002/bit.23216.

98. Yang, Y., Mariati, Chusainow, J., Chusainow, J., and Yap, M.G.S. (2010). DNA methylation contributes to loss in productivity of monoclonal antibody-producing CHO cell lines. J. Biotechnol. *147*, 180–185. https://doi.org/10.1016/j.jbiotec.2010.04.004.

99. Kravitz, A.V., Freeze, B.S., Parker, P.R.L., Kay, K., Thwin, M.T., Deisseroth, K., and Kreitzer, A.C. (2010). Regulation of parkinsonian motor behaviours by optogenetic control of basal ganglia circuitry. Nature *466*, 622–626. https://doi.org/10.1038/nature09159.

100. Wertz, A., Trenholm, S., Yonehara, K., Hillier, D., Raics, Z., Leinweber, M., Szalay, G., Ghanem, A., Keller, G., Rózsa, B., et al. (2015). PRESYNAPTIC NETWORKS. Single-cell-initiated monosynaptic tracing reveals layer-specific cortical network modules. Science *349*, 70–74. https://doi.org/10.1126/science.aab1687.

101. Gompf, H.S., Budygin, E.A., Fuller, P.M., and Bass, C.E. (2015). Targeted genetic manipulations of neuronal subtypes using promoter-specific combinatorial AAVs in wild-type animals. Front. Behav. Neurosci. *9*, 152. https://doi.org/10.3389/fnbeh.2015.00152.

102. Stauffer, W.R., Lak, A., Yang, A., Borel, M., Paulsen, O., Boyden, E.S., and Schultz, W. (2016). Dopamine Neuron-Specific Optogenetic Stimulation in Rhesus Macaques. Cell *166*, 1564–1571.e6. https://doi.org/10.1016/j.cell.2016.08.024.

103. O'Shea, D.J., Kalanithi, P., Ferenczi, E.A., Hsueh, B., Chandrasekaran, C., Goo, W., Diester, I., Ramakrishnan, C., Kaufman, M.T., Ryu, S.I., et al. (2018). Development of an optogenetic toolkit for neural circuit dissection in squirrel monkeys. Sci. Rep. *8*, 6775. https://doi.org/10.1038/s41598-018-24362-7.

104. Gill, D.R., Smyth, S.E., Goddard, C.A., Pringle, I.A., Higgins, C.F., Colledge, W.H., and Hyde, S.C. (2001). Increased persistence of lung gene expression using plasmids containing the ubiquitin C or elongation factor 1alpha promoter. Gene Ther. *8*, 1539–1546. https://doi.org/10.1038/sj.gt.3301561.

105. Gopalkrishnan, R.V., Christiansen, K.A., Goldstein, N.I., DePinho, R.A., and Fisher, P.B. (1999). Use of the human EF-1alpha promoter for expression can significantly increase success in establishing stable cell lines with consistent expression: a study using the tetracycline-inducible system in human cancer cells. Nucleic Acids Res. *27*, 4775–4782. https://doi.org/10.1093/nar/27.24.4775.

106. Teschendorf, C., Warrington, K.H., Jr., Siemann, D.W., and Muzyczka, N. (2002). Comparison of the EF-1 alpha and the CMV promoter for engineering stable tumor cell lines using recombinant adeno-associated virus. Anticancer Res. *22*, 3325–3330.

107. Yamazaki, Y., Hirai, Y., Miyake, K., and Shimada, T. (2014). Targeted gene transfer into ependymal cells through intraventricular injection of AAV1 vector and long-term enzyme replacement via the CSF. Sci. Rep. *4*, 5506. https://doi.org/10.1038/srep05506.

108. Mathiesen, S.N., Lock, J.L., Schoderboeck, L., Abraham, W.C., and Hughes, S.M. (2020). CNS Transduction Benefits of AAV-PHP.eB over AAV9 Are Dependent on Administration Route and Mouse Strain. Mol. Ther. Methods Clin. Dev. *19*, 447–458. https://doi.org/10.1016/j.omtm.2020.10.011.

109. Albright, B.H., Storey, C.M., Murlidharan, G., Castellanos Rivera, R.M., Berry, G.E., Madigan, V.J., and Asokan, A. (2018). Mapping the Structural Determinants Required for AAVrh.10 Transport across the Blood-Brain Barrier. Mol. Ther. *26*, 510–523. https://doi.org/10.1016/j.ymthe.2017.10.017.

STAR★METHODS

KEY RESOURCES TABLE

REAGENT or RESOURCE	SOURCE	IDENTIFIER
Antibodies		
mouse anti-GAPDH	Proteintech	Cat# 60004-1-Ig; RRID: AB_2107436
goat anti-CathD	R&D Systems	Cat# AF1029; RRID: AB_2087094
goat anti-human PGRN	R&D Systems	Cat# AF2420; RRID: AB_2114489
sheep anti-mouse PGRN	R&D Systems	Cat# AF2557; RRID: AB_2114504
mouse anti-CHAT	R&D Systems	Cat# AF3447
mouse anti-NeuN	Millipore	Cat# MAB377; RRID: AB_2298772
mouse anti-GFAP (GA5)	Cell Signaling Technology	Cat# 3670S; RRID: AB_561049
rabbit anti-IBA-1	Wako	Cat# 01919741; RRID: AB_839504
goat anti-IBA1	Novus Biologicals	Cat# NB100-1028; RRID: AB_521594
rat anti-CD68	Bio-Rad	Cat# MCA1957; RRID: AB_322219
rabbit anti-p62	MBL	Cat# PM045; RRID: AB_1279301
rat anti-phospho TDP43 (Ser409/Ser410)	Millipore	Cat# MABN14; RRID: AB_11212279
mouse anti-Ubiquitin	BioLegend	Cat# 646302; RRID: AB_1659269
rabbit anti-TMEM106B	Home-made	Brady, 2013
rabbit anti-human granulin E	Home-made	This paper
IRDye 800CW Donkey anti-Mouse IgG	LI-COR Biosciences	Cat# 926-32212; RRID: AB_621847
IRDye 800CW Donkey anti-Rabbit IgG	LI-COR Biosciences	Cat# 926-32213; RRID: AB_621848
Donkey anti-Goat IgG Alexa Fluor 800	Thermo Fisher Scientific	Cat# A-21084; RRID: AB_2535741
Donkey anti-Rabbit IgG Alexa Fluor 680	Thermo Fisher Scientific	Cat# A10043; RRID: AB_2534018
Donkey anti-Mouse IgG Alexa Fluor 680	Thermo Fisher Scientific	Cat# A10038; RRID: AB_2534014
Donkey anti-Mouse IgG Alexa Fluor 488	Thermo Fisher Scientific	Cat# A21202; RRID: AB_141607
Donkey anti-Mouse IgG Alexa Fluor 594	Thermo Fisher Scientific	Cat# A21209; RRID: AB_2535795
Donkey anti-Rabbit IgG Alexa Fluor 568	Thermo Fisher Scientific	Cat# A10042; RRID: AB_2534017
Donkey anti-Rabbit IgG Alexa Fluor 647	Jackson ImmunoResearch Laboratories	Cat# 711-605-152; RRID: AB_2492288
Donkey anti-Mouse IgG Alexa Fluor 647	Jackson ImmunoResearch Laboratories	Cat# 715-605-150; RRID: AB_2340862
Donkey anti-Sheep IgG Alexa Fluor 680	Jackson ImmunoResearch Laboratories	Cat# 713-625-147; RRID: AB_2340753
Donkey anti-Goat IgG Alexa Fluor 488	Thermo Fisher Scientific	Cat# A11055; RRID: AB_2534102
Donkey anti-Goat IgG Alexa Fluor 594	Thermo Fisher Scientific	Cat# A11058; RRID: AB_2534105
Donkey anti-Goat IgG Alexa Fluor 647	Thermo Fisher Scientific	Cat# A21447; RRID: AB_2535864
Donkey anti-rat IgG Alexa Fluor 594	Jackson ImmunoResearch Laboratories	Cat# 712-585-153; RRID: AB_2340689
Donkey anti-mouse IgG Alexa Fluor 488	Jackson ImmunoResearch Laboratories	Cat# 715-545-151; RRID: AB_2341099
Critical commercial assays		
Human Progranulin DuoSet ELISA Kit	R&D Systems	Cat# DY2420
Cone-bottom collection tube	Sarstedt	Cat# 41.1500.005
TrueBlack Lipofuscin Autofluorescence Quencher	Biotium	Cat# 23007
Odyssey blocking buffer	LI-COR Biosciences	Cat# 927-40000
protease inhibitor	Roche	Cat# 05056489001
Pierce BCA Protein Assay Kit	Thermo Fisher Scientific	Cat# 23225
O.C.T compound	Electron Microscopy Sciences	Cat# 62550-01

(*Continued on next page*)

Continued

REAGENT or RESOURCE	SOURCE	IDENTIFIER
Experimental models: Cell lines		
Lec2 cells	ATCC	Cat# CRL-1736
HEK293T cells	ATCC	Cat# CRL-1573
Experimental models: Organisms/strains		
Mouse: C57BL/6	Jackson Laboratory	RRID: IMSR_JAX:000664
Mouse: *Grn*$^{-/-}$ C57BL/6	Jackson Laboratory	RRID: IMSR_JAX:013175
Mouse: *Tmem106b*$^{-/-}$ C57BL/6	Feng et al. 2020	N/A
Bacterial and virus strains		
AAV1-hPGRN	Alector	This paper
AAV9-hPGRN	Alector	This paper
Software and algorithms		
Viewer III Software	Biobserve, Bonn, Germany	N/A
GraphPad Prism 9	Graphpad Software	https://www.graphpad.com/
ImageJ	NIH	N/A
Image Studio Lite	LI-COR Biosciences	N/A
SlideBook 6	Intelligent Imaging Innovations, Inc.	N/A

RESOURCE AVAILABILITY

Lead contact

Further information and requests for resources and reagents should be directed to and will be fulfilled by the lead contact, FenghuaHu (fh87@cornell.edu).

Materials availability

Plasmids generated in this study are available from the lead contact upon request.

Data and code availability

- Data reported in this paper and any additional information required to reanalyze the data reported in this paper are available from the lead contact upon request.
- This paper does not report any original code.
- All other items are available from the lead contact upon request.

EXPERIMENTAL MODEL AND STUDY PARTICIPANT DETAILS

Mouse strains

Tmem106b$^{-/-}$ mice (Δ341bp) were generated using the CRISPR/Cas9 gene editing technique.[98] C57BL/6 and *Grn*$^{-/-}$ mice[25] were obtained from the Jackson laboratory. *Tmem106b*$^{-/-}$ × *Grn*$^{-/-}$ mating was used to produce *Tmem106b*$^{+/-}$*Grn*$^{+/-}$ mice. *Tmem106b*$^{+/-}$*Grn*$^{-/-}$ or *Tmem106b*$^{-/-}$*Grn*$^{+/-}$ mice were obtained from *Tmem106b*$^{+/-}$*Grn*$^{+/-}$ × *Tmem106b*$^{+/-}$*Grn*$^{+/-}$ mating and *Tmem106b*$^{-/-}$*Grn*$^{-/-}$ mice were obtained from *Tmem106b*$^{+/-}$*Grn*$^{-/-}$ × *Tmem106b*$^{+/-}$*Grn*$^{-/-}$ or *Tmem106b*$^{-/-}$*Grn*$^{+/-}$ × *Tmem106b*$^{-/-}$*Grn*$^{+/-}$ mating. All animals (1-6 adult mice per cage) were housed in a 12h light/dark cycle. Mixed male and female mice were used for this study. The age of the mice used in each experiment is indicated in the figure legend. The animal protocol (2017-0056) was approved by Cornell University's animal care and use committee following the National Research Council's guide to the care of laboratory animals.

AAV plasmids, capsids, and testing

The AAV-*GRN* transgene (ssAAV-EF1a-Kozak-hPGRN-WPRE-hGHpA) was generated by cloning a codon-optimized human *GRN* cDNA into a single-stranded AAV vector containing a human EF1a promoter. A human growth hormone poly(A) sequence was added to increase mRNA stability, a Kozak sequence was added for efficient initiation of translation, and the woodchuck hepatitis virus posttranscriptional

regulatory element (WPRE) was incorporated to enhance PGRN expression.Plasmid preparation was performed by GenScript and Aldevron, and plasmids were tested for effective PGRN expression and secretion by transfecting HEK293 and Lec2 cells and measuring intracellular PGRN (using lysed cells) and secreted PGRN (using conditional medium) via ELISA (R&D Systems kit).

The ssAAV-*GRN*transgene was packaged into AAV1 and AAV9 capsids by Viralgen and AAV were tested for effective PGRN expression and secretion by transducing Lec2 cells and measuring intracellular PGRN (using lysed cells) and secreted PGRN (using conditional medium) via ELISA (R&D Systems kit).

METHOD DETAILS

Stereotactic injection of AAV

Mice were anesthetized with inhalation of isoflurane and mounted on a stereotactic device. Excipient control buffer (10 mM Phosphate, 138mM NaCl, 2.7 mM KCl, & 0.001% Pluronic-68), AAV1 or AAV9 particles containing human *Grn* gene at the dose of 3.02 or 3.11×10^{13} vector genomes (vg)/mL were stereotactically injected bilaterally into lateral ventricles (ICV) of 6-week- or 9-week-old *Tmem106b*$^{-/-}$*Grn*$^{-/-}$ mice (2 μL/injection/site at the rate of 0.2 μL/min). Stereotactic coordinates of injection sites from bregma were as follows: −0.3 anterior/posterior, ±1.0 medial/lateral, and 1.6 dorsal-ventral relative to bregma (in millimeters). Mice were sacrificed at 5 months of age, and brain and spinal cord samples were dissected for immunohistochemistry and biochemical analyses.

Behavioral test

2-3 days before sacrificing, all the mice were subjected to the following behavioral tests.(1) Open-field test: Mice were placed in a clear plastic chamber (40 × 40 × 40 cm) for 10 min. Total movements in the open field were automatically recorded by the Viewer III software (Biobserve, Bonn, Germany). The apparatus was thoroughly cleaned with 70% ethanol. (2) Hindlimb clasping test: Briefly, mice were suspended by the base of the tail and their behaviors were recorded for 30 seconds by the Viewer III software (Biobserve, Bonn, Germany). (3) Rolling over test: The mice were flipped back, and the time for the mice to flip back was recorded with a video camera. Five measurements with an intertrial interval of 1 min were performed. (4) Footprint test: The footprint apparatus consists of a runway (50 cm in length), with a dark box at the end. Mice are trained to walk straight to the dark box on the white paper before the trial. The hind paws of the mice are painted with blue color. Then the mice are made to walk on the white paper. The footprint pattern is analyzed for stride length. Stride length is determined by measuring the distance between each step of the same side of the body. For all behavioral analyses, experimenters were blind to the genotypes of the mice.

Tissue preparation for western blot analysis

Mice were perfused with 1× PBS and tissues were dissected and snap-frozen with liquid nitrogen and kept at −80°C. On the day of the experiment, frozen tissues were thawed and homogenized on ice with bead homogenizer (Moni International) in ice-cold RIPA buffer (150 mM NaCl, 50 mM Tris-HCl (pH 8.0), 1% Triton X-100, 0.5% sodium deoxycholate, 0.1% SDS) with 1 mM PMSF, proteinase and phosphatase inhibitors. After centrifugation at 14,000 × g for 15 minutes at 4°C, supernatants were collected as the RIPA-soluble fraction. The insoluble pellets were washed with RIPA buffer and extracted in 2× v/w of urea buffer (7 M Urea, 2 M Thiourea, 4% CHAPS, 30 mM Tris, pH 8.0). After sonication, samples were centrifuged at 200,000 × g at 24°C for 1 hour, and the supernatant was collected as the urea-soluble fraction. Protein concentrations were determined via BCA assay, then standardized. Equal amounts of protein were analyzed by western blot using the indicated antibodies.

Human PGRN ELISA

To determine the human PGRN levels in the serum, frontal cortex, and spinal cord lysates, homemade rabbit anti-human granulin E antibodies were used to coat a 96-well microplate with 100 μL per well and incubate overnight at 4°C. The next day, after washing with 250 μl washing buffer (0.05% Tween® 20 in PBS, pH 7.4) for 3 min, the wells were blocked with blocking buffer (1% BSA in PBS, pH 7.4) for 1 hour, followed by incubation with the proper amount of samples or recombinant PGRN protein (Human Progranulin DuoSet ELISA, R&D Systems) at concentrations of 62.5, 125, 250, 500, 1000, 2000 and 4000 pg/mL for 2 hours. The wells were then washed three times before incubation with the detection Antibody (Human Progranulin DuoSet ELISA, R&D Systems) for 2 hours. Then the plate was incubated with Streptavidin-HRP solution

for 20 minutes at room temperature. After 3 washes, 50 μL of TMB substrate solution (Thermo Fisher Scientific) was added into the wells and the plate was incubated for 5–15 min until blue color appeared. The reaction was stopped with 2N H_2SO_4 solution (Thermo Fisher Scientific). The optical density was determined by a microplate reader using the readings at 450 nm and subtracting the readings at 540 nm.

Immunofluorescence staining

Mice were perfused with cold PBS and tissues were post-fixed with 4% paraformaldehyde. After dehydration in 30% sucrose buffer, tissues were embedded in O.C.T compound (Electron Microscopy Sciences).15-μm-thick sections were blocked and permeabilized with either 0.1% saponin in Odyssey blocking buffer or 0.2% Triton X-100 in 1× PBS with 10% horse serum before incubating with primary antibodies overnight at 4°C. The next day, sections were incubated with secondary fluorescent antibodies at room temperature for 1 hour. After fluorescence immunolabeling, the sections were stained with Hoechst and then mounted using a mounting medium (Vector laboratories). To block the autofluorescence, all sections were incubated with 1× TrueBlack Lipofuscin Autofluorescence Quencher (Biotium) in 70% ethanol for 30 seconds at room temperature before or after the staining process. Antigen retrieval was performed by microwaving the sections in sodium citrate buffer (pH 6.0) for 15 min.

Image acquisition and analysis

Images were acquired on a CSU-X spinning disc confocal microscope (Intelligent Imaging Innovations) with an HQ2 CCD camera (Photometrics) using 40x, 63x, and 100x objectives. Eight to ten different random images were captured, and the fluorescence intensity was measured directly with ImageJ after a threshold application. Lower magnification images were captured by 4x, 10x, or 20x objectives on a Leica DMi8 inverted microscope. The fluorescence intensity was measured directly with ImageJ after a threshold application. Data from $\geq$3 brains in each genotype were used for quantitative analysis.

QUANTIFICATION AND STATISTICAL ANALYSIS

All statistical analyses were performed using GraphPad Prism 8. All data are presented as mean $\pm$ SEM. Statistical significance was assessed by unpaired Student's *t* test (for two groups comparison), and one-way ANOVA tests with Tukey's multiple comparisons (for multiple comparisons). p values less than or equal to 0.05 were considered statistically significant. *$p < 0.05$; **$p < 0.01$; ***$p < 0.001$; ****$p < 0.0001$.